Fundamental Issues and Recent Advancements in Analysis of Aircraft Brake Natural Convective Cooling

M. P. Dyko
Research and Technology,
Aircraft Braking Systems Corporation,
Akron, OH 44306
Mem. ASME

K. Vafai[1]
Department of Mechanical Engineering,
The Ohio State University,
Columbus, OH 43210
vafai.1@osu.edu
Fellow ASME

A heightened awareness of the importance of natural convective cooling as a driving factor in design and thermal management of aircraft braking systems has emerged in recent years. As a result, increased attention is being devoted to understanding the buoyancy-driven flow and heat transfer occurring within the complex air passageways formed by the wheel and brake components, including the interaction of the internal and external flow fields. Through application of contemporary computational methods in conjunction with thorough experimentation, robust numerical simulations of these three-dimensional processes have been developed and validated. This has provided insight into the fundamental physical mechanisms underlying the flow and yielded the tools necessary for efficient optimization of the cooling process to improve overall thermal performance. In the present work, a brief overview of aircraft brake thermal considerations and formulation of the convection cooling problem are provided. This is followed by a review of studies of natural convection within closed and open-ended annuli and the closely related investigation of inboard and outboard subdomains of the braking system. Relevant studies of natural convection in open rectangular cavities are also discussed. Both experimental and numerical results obtained to date are addressed, with emphasis given to the characteristics of the flow field and the effects of changes in geometric parameters on flow and heat transfer. Findings of a concurrent numerical and experimental investigation of natural convection within the wheel and brake assembly are presented. These results provide, for the first time, a description of the three-dimensional aircraft braking system cooling flow field.

Introduction

The combined worldwide sales of wheels and brakes for transport, commuter, business, and military aircraft now exceeds one billion dollars annually. A large segment of the aircraft in the world commercial fleet fly short-haul routes which require rapid cooling of the brakes after landing in order to prevent operational delays. Forced convection air flow is sometimes utilized to reduce cooling times, but there are significant penalties associated with the axle mounted fans employed for this purpose including increased weight and higher cost. For this reason, cooling by means of buoyancy-induced air flow is relied upon in most cases. It is recognized that augmentation of heat dissipation through enhanced natural convection heat transfer offers the potential to increase aircraft revenue flying time and in some cases eliminate the need for axle fans. Current trends in aircraft brake performance requirements of shorter aircraft turnaround time (Currey, 1988), increased heat sink energy loading, and lighter weight (Greenbank, 1991) have resulted in greater focus on maximizing heat loss from the system. As an important step toward developing production design methods to improve cooling performance, numerical simulations of braking system natural convection flow fields as described in this paper have been developed and employed in cooling optimization studies.

In an aircraft wheel and brake assembly, which is shown schematically in Fig. 1, multiple carbon-carbon composite or metallic rotating and stationary disks are grouped together in a subassembly known as the brake heat sink or brake stack. The frictional force necessary to stop the aircraft is developed at the interfaces between the rotors and stators when they are clamped together by the brake pistons, which in nearly all designs are actuated hydraulically. During the main braking event following touchdown, a major portion of the aircraft kinetic energy is converted to thermal energy at these friction interfaces and absorbed by the rotors and stators. After this brake application and subsequent lower speed applications during taxi-in to the gate, the aircraft comes to a stop and remains stationary for a relatively long period. During this time, a significant amount of the heat sink stored energy is removed directly by natural convection air flow in the annular space between the brake stack and wheel as well in the regions adjacent to the ends of the brake stack/frame subassembly. Brake stack heat is also transferred directly and indirectly by thermal radiation and conduction to surrounding components such as the wheel, piston housing subassembly, and axle, which in turn dissipate heat to the surroundings. Radiation heat loss also occurs directly from the brake stack to the environment. Natural convection currents that develop in the open annular cavity formed by the wheel outboard surfaces are responsible for much of the total heat dissipated by the wheel. The combined processes of energy absorption, redistribution, and dissipation determine the overall system thermal response, which to a significant degree is dependent on natural convection.

During brake application, the average rate of energy absorption is much greater than the combined rate of heat loss from the brake disks due to convection, radiation, and conduction. Therefore the mean temperature of the heat sink at the end of the stop is essentially a function of the thermal capacitance of

[1] To whom correspondence should be addressed.

Contributed by the Heat Transfer Division for publication in the JOURNAL OF HEAT TRANSFER. Manuscript received by the Heat Transfer Division, June 25, 1998. Keywords: Augmentation, Computational, Conjugate, Experimental, Heat Transfer, Natural Convection. Associate Technical Editor: Y. Jaluria.

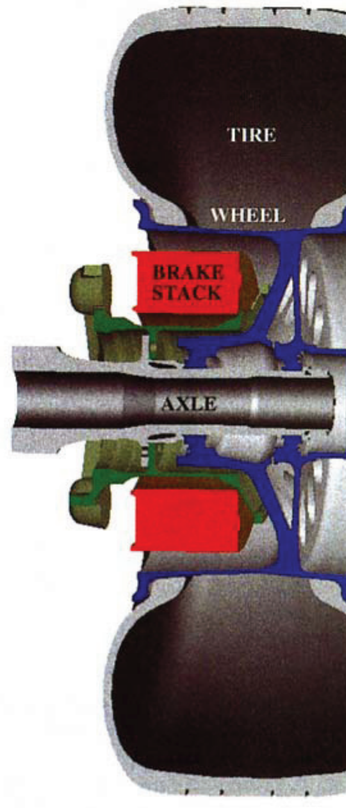

Fig. 1 Schematic of an aircraft wheel and brake assembly, axle, and tire

the heat sink, the total energy absorbed by the brake, and the initial temperature of the brake disks. For steel disk-type aircraft brakes, which have been in widespread use for over 35 years, heat sink mean temperatures up to approximately 1400°F are possible during short-haul commercial operation, while temperatures exceeding the melting point of the friction material can occur locally for the rejected take-off condition. Carbon-carbon composite brake disks were first introduced in the 1960s and are now commonly used, offering much greater energy absorption capability per pound than steel. The thermal environment for carbon brakes is more severe than steel, with heat sink mean temperatures as high as approximately 1800°F occurring under conditions of heavy usage. Peak temperatures at the carbon disk friction interfaces may exceed 3500°F under worst-case conditions.

The high temperatures attained by the heat sink require careful implementation of system thermal management methods in order to prevent strength loss and/or damage of the braking system and landing gear components. The US Patent literature dealing with thermal barrier technology and other methods developed specifically for controlling aircraft brake heat transfer is substantial, highlighting the major challenges that are present. Examples of thermal management features commonly incorporated into the braking system include wheel ventilation holes to promote convection cooling, heat shields to reduce radiation heat transfer to the wheel and axle, beam-type wheel drive keys to reduce heat conduction into the wheel, and insulators to minimize conduction into the piston housing subassembly and axle. In general, the number and types of thermal barriers are selected to reduce heating of the components surrounding the brake stack to acceptable levels while at the same time maintaining sufficient cooling of the brake stack.

Examples of thermally related problems due to insufficient heat capacity, thermal barrier protection, or cooling include release of wheel fusible plugs (which prevents overpressurization of the tire) at unacceptably low energy levels, strength reduction of the aluminum wheel, degradation of hydraulic seals and hydraulic fluid properties, deterioration of tire rubber, and damage to the axle. Under conditions involving misuse of the brakes, tire fire can occur and heat-related failures leading to leakage of hydraulic fluid and subsequent fluid fire

Nomenclature

- b = annular gap width = $r_o - r_i$
- c_p = specific heat of fluid
- c_{pw} = specific heat of solid wall
- $\mathbf{e}$ = unit gravitational vector = $\cos\theta \mathbf{e}_1 - \sin\theta \mathbf{e}_2$
- g = gravitational acceleration
- $\mathbf{g}$ = gravitational vector = $-g\mathbf{e}$
- h = heat transfer coefficient
- k = turbulent kinetic energy
- L = length to radius ratio = l_2/r_i
- l_c = characteristic length
- l_e = length of extended computational domain
- l_1 = length of wheel outboard cavity
- l_2 = length of brake stack
- l_3 = distance between brake stack and z datum
- Nu = Nusselt number = hr_o/λ
- Nu_{av} = average Nusselt number
- Pr = Prandtl number = ν/α
- Pr_t = turbulent Prandtl number
- n = outward normal from surface
- p = pressure
- q = applied heat flux
- R = radius ratio = r_o/r_i
- Ra = Rayleigh number based on annular gap width = $g\beta(T_i - T_{\mathrm{ref}})b^3/\alpha\nu$
- Ra_{ro} = Rayleigh number based on outer radius = $g\beta(T_i - T_{\mathrm{ref}})r_o^3/\alpha\nu$
- Ra_{ri} = Rayleigh number based on inner radius = $g\beta(T_i - T_{\mathrm{ref}})r_i^3/\alpha\nu$
- Ra_{ro}^* = modified Rayleigh number = $g\beta q r_o^4/\lambda\alpha\nu$
- r = radial coordinate
- r_e = radius of extended computational domain
- r_i = radius of inner cylinder
- r_{ih} = radius of wheel hub
- r_o = radius of outer cylinder
- r_s = inner radius of brake stack end wall
- T = temperature
- T_i = temperature at surface of inner cylinder
- T_{ref} = reference temperature
- T_w = temperature of solid wall
- T_∞ = ambient temperature
- t_w = thickness of wheel web
- U = characteristic velocity = $(\alpha/r_o)\sqrt{\mathrm{Ra}_r^*\,\mathrm{Pr}}$
- u_r = radial velocity
- u_θ = angular velocity
- u_z = axial velocity
- $\mathbf{u}$ = velocity vector
- z = axial coordinate

Greek Symbols

- α = thermal diffusivity
- β = volume expansion coefficient
- δ = height of the wall element
- ε = dissipation of turbulent kinetic energy
- κ = Von Karman constant
- λ = thermal conductivity of fluid
- λ_{eff} = effective thermal conductivity
- λ_t = turbulent thermal conductivity
- λ_w = thermal conductivity of wall
- μ = dynamic viscosity
- μ_{eff} = effective viscosity
- μ_t = turbulent viscosity
- ν = kinematic viscosity
- θ = angular coordinate
- τ = stress tensor
- τ_{eff} = effective stress tensor

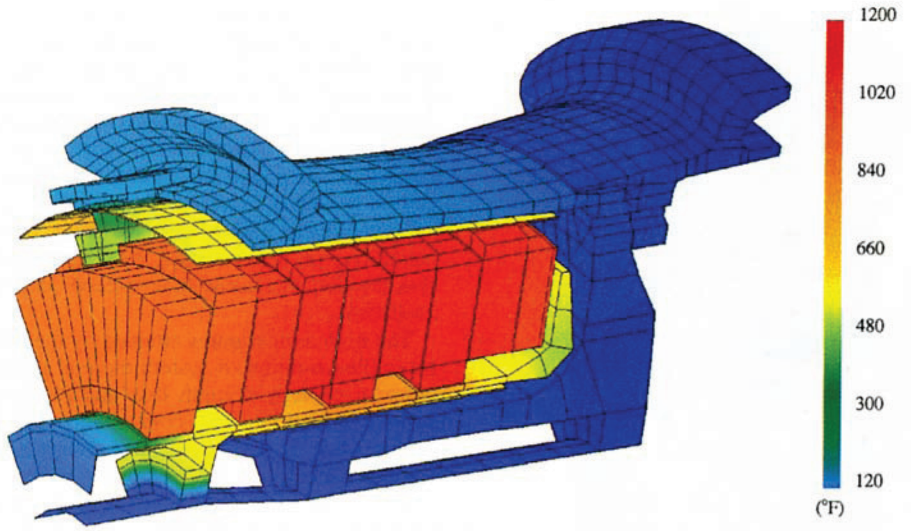

Fig. 2 Wheel and brake temperature distribution eight minutes after a high energy stop (from Dyko and Chung, 1990)

are possible, thus posing a potential threat to safety. Hence, in addition to directly affecting aircraft turnaround time which is a critical performance parameter, the influence of natural convection cooling on overall system thermal behavior profoundly impacts the reliability and safety of the braking system. In addition to these issues, a major objective in the design of aircraft braking systems is to minimize assembly weight. Reducing the weight of the braking system increases the difficulty of the thermal management problem and makes it imperative to understand the net benefits to be obtained from altering the design for increased convective heat loss. Our increased understanding of natural convection cooling for fundamental braking system geometries positively impacts each of the above cited issues.

To help ensure that a new design will meet thermal requirements and to analyze changes to existing designs, numerical heat transfer models are employed to predict the transient temperature distributions within wheel and brake components. Computer codes tailored specifically for simulation of braking system multimode heat transfer are used by the manufacturers of aircraft brakes. Typically, thermal network principles which are analogous to resistance-capacitance electrical networks and can be flexibly applied to a wide range of wheel and brake configurations are followed. The finite element method has also been applied to the multicomponent braking system heat transfer problem with good success (Dyko and Chung, 1990), offering greater resolution of thermal gradients within the individual components. An example of wheel and brake temperature distributions calculated with this method is provided in Fig. 2 for a time of eight minutes after a high-energy braking event. With both the thermal network and finite element models, peak temperatures and cooling times for established brake configurations can be predicted quite accurately. However, the heat transfer coefficient relations employed in convective boundary conditions have traditionally been empirically based and thus restrict the ability to study the effects of changes in geometry on convection cooling. Therefore, it is necessary to analyze the braking system natural convection air flow and temperature fields to obtain improved predictions of heat transfer for new designs and to better evaluate design changes for increased cooling rates. Convective heat transfer correlations for the different regions of the braking system have been successfully developed from results of recent numerical and experimental studies of brake stack/wheel subdomain and wheel and brake assembly flow fields that are described herein. An example of results obtained by integrating the correlations into a thermal model of the braking system and the close agreement of these results with experimental data is presented in a later section. A summary of the available correlations is provided in Table 1.

The aircraft wheel and brake assembly shown schematically in Fig. 1 is comprised of the brake stack and brake frame, wheel inboard and outboard halves, and piston housing subassembly. These components are supported by the axle which attaches to the landing gear strut. It is evident from this diagram that the air passages within the braking system consist primarily of (a) an open-ended horizontal annulus bounded at its inner diameter by the brake stack and at its outer diameter by the wheel (brake stack/wheel subdomain), (b) an open-ended horizontal annular cavity formed by the wheel outboard surfaces (wheel outboard subdomain), and (c) connecting regions between these two subdomains defined by the wheel web ventilation passages (distributed circumferentially around the web) and the web itself. The system is

Table 1 Summary of available Nusselt number correlations for the braking system

Wheel Outboard Region

$$(1.27 \times 10^9 \leq Ra^*_{ro} \leq 5.05 \times 10^9)$$

$$Nu_{av} = 0.0136\ (Ra^*_{ro})^{0.376} \quad \text{(outer cylinder)} \tag{29}$$

$$Nu_{av} = 0.0133\ (Ra^*_{ro})^{0.379} \quad \text{(end wall)} \tag{30}$$

$$Nu_{av} = 0.0113\ (Ra^*_{ro})^{0.381} \quad \text{(inner cylinder)} \tag{31}$$

$$Nu_{av} = 0.0119\ (Ra^*_{ro})^{0.378} \quad \text{(inner cylinder tip)} \tag{32}$$

$$Nu_{av} = 0.0131\ (Ra^*_{ro})^{0.378} \quad \text{(cavity)} \tag{33}$$

Brake Stack

$$Nu_{av} = 0.134\ (Ra^*_{ro})^{0.264}\text{: } 7.09 \times 10^8 \leq Ra^*_{ro} \leq 4.76 \times 10^9 \tag{34}$$

$$Nu_{av} = 0.2\ (Ra_{ri})^{0.14}(1 - 0.705L)[1 + 27.74(R - 1)]\text{:} \quad Ra_{ri} < 1 \times 10^5 \tag{35}$$

$$Nu_{av} = 0.2\ (Ra_{ri})^{0.174}(1 - 0.525L)[1 + 28.01(R - 1)]\text{:} \quad 1 \times 10^5 \leq Ra_{ri} \leq 1 \times 10^6 \tag{36}$$

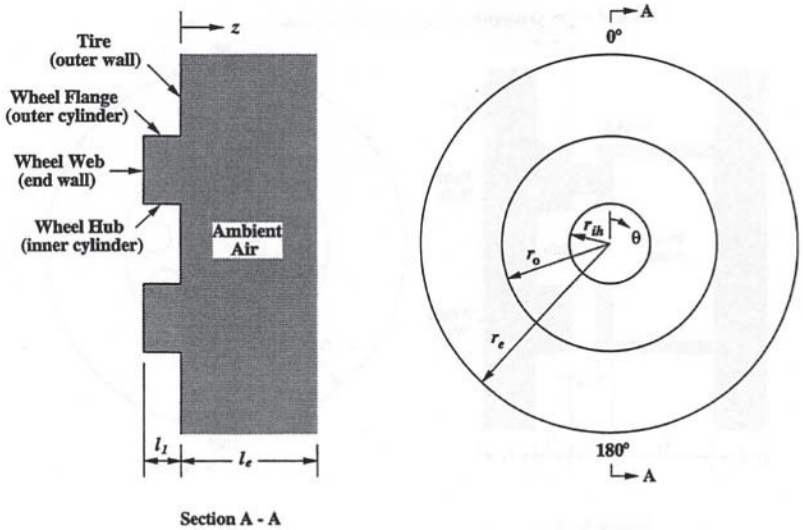

Fig. 3 Wheel outboard subdomain

cooled by ambient air outside the assembly, which enters the internal regions through the open ends of the brake stack/wheel and wheel outboard subdomains. The air subsequently gains energy from the brake stack and from surrounding wheel and brake components which are heated by the stack, and returns to the external region through these open ends. For the purposes of convective heat transfer analysis, the cooling passage geometries associated with the wheel and brake assembly are modeled for the general case as wheel outboard and brake stack/wheel subdomains and the overall wheel and brake assembly domain as shown in Figs. 3–5. From these geometries, it is apparent that studies of natural convection within the wheel outboard, brake stack/wheel, and overall wheel and brake assembly (combined inboard and outboard) regions have their basis in the more fundamental investigation of buoyancy-driven flow and heat transfer within closed and open-ended horizontal annuli.

As discussed in this paper, the fundamental work pertaining to basic horizontal annuli has recently been expanded to consider the higher Rayleigh numbers associated with an aircraft brake, annulus aspect ratios corresponding to actual wheel and brake geometries, conjugate heat transfer, thermal boundary conditions more closely representative of a braking system, and the simultaneous interaction of wheel outboard and brake stack/wheel flow fields with each other and the external flow field. These fundamental and practical advancements have resulted in a much more realistic simulation of three-dimensional aircraft braking system buoyancy induced cooling. Several significant challenges associated with optimizing aircraft brake cooling still lie ahead, however. These include incorporating more detailed design features into the wheel and brake assembly simulation and establishing the braking system design trade-offs associated with enhanced cooling configurations.

The review section of this paper, which follows presentation of the governing equations and boundary conditions, is divided into two main parts. The first part (Fundamental Advancements) addresses pertinent fundamental studies which lay the groundwork for the practical experimental and numerical work discussed in the second part (Braking System Subdomains). Following this, results of the current investigation of natural convection within the overall wheel and brake assembly are presented (Wheel and Brake Assembly). The fundamental work provides the reader with a solid understanding of the underlying

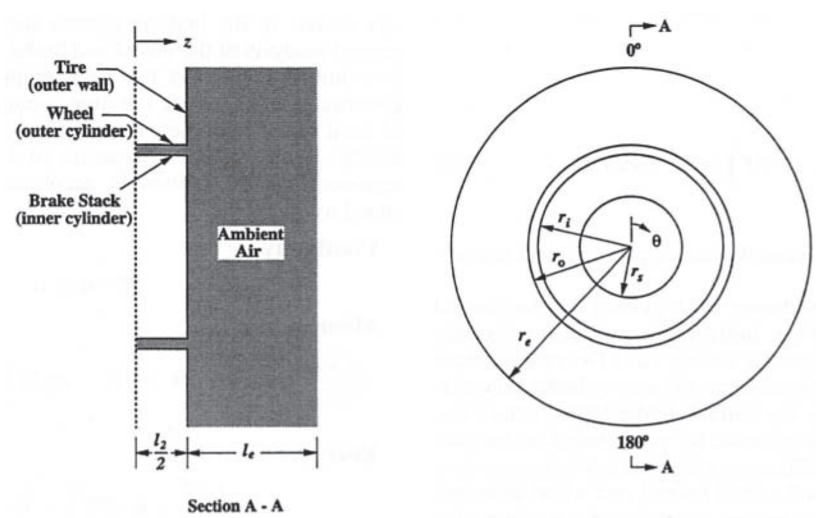

Fig. 4 Brake stack/wheel subdomain

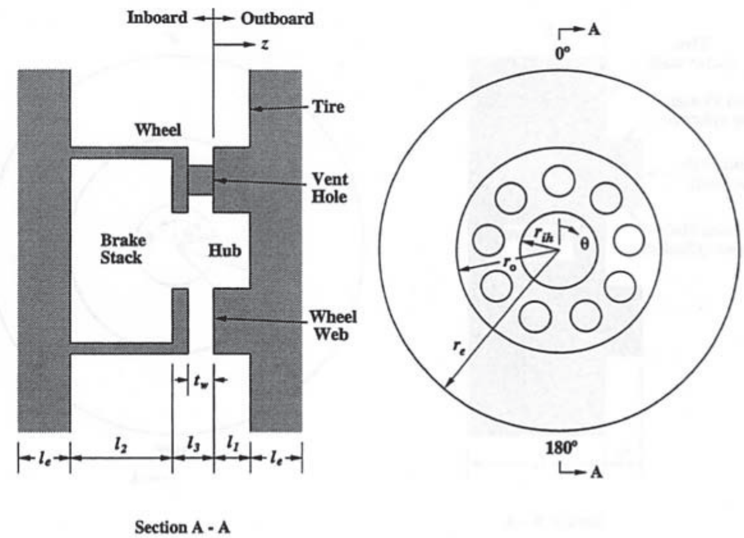

Fig. 5 Wheel and brake assembly domain

convective flow processes prior to attempting to understand the more complicated flows associated with the actual braking system geometry.

Governing Equations

In order to clearly distinguish fundamental characteristics of the three-dimensional cooling flows and efficiently analyze the effects of changes in geometry on cooling performance, it is usually assumed that (a) the fluid is Newtonian, (b) viscous dissipation is negligible, and (c) in accordance with the Boussinesq approximation, density is constant except when it directly causes buoyancy forces. Based on these assumptions, the governing equations can be written as follows.

Continuity.

$$\nabla \cdot \mathbf{u} = 0 \tag{1}$$

Momentum.

$$\rho\left(\frac{\partial \mathbf{u}}{\partial t} + \mathbf{u} \cdot \nabla \mathbf{u}\right) = -\nabla p - \rho \mathbf{g} \beta (T - T_\infty) + \nabla \cdot \tau \tag{2}$$

Energy.

$$\rho c_p\left(\frac{\partial T}{\partial t} + \mathbf{u} \cdot \nabla T\right) = \nabla \cdot (\lambda \nabla T) \tag{3}$$

where $\mathbf{u}$, p, and T, are the velocity vector, pressure, and temperature, respectively.

It has been shown by Mahoney et al. (1986) that for natural convection of gases between horizontal concentric cylinders, the Boussinesq approximation is strictly valid for a temperature difference ratio (defined as the inner to outer cylinder temperature difference divided by the outer cylinder temperature) less than 0.1 and is reasonably accurate for predicting heat transfer rates up to a temperature difference ratio of 0.2. The temperature difference ratios for the brake stack/wheel and wheel outboard subdomains of the braking system meet the above criteria for validity of the Boussinesq approximation for a wide range of typical brake operating conditions. Furthermore, the agreement of results from numerical models which employ this approximation with test data is very good as shown in Vafai et al. (1997) and Desai and Vafai (1996) for the brake stack/wheel and wheel outboard subdomains, respectively. Under severe brake operating conditions the Boussinesq approximation is not strictly satisfied, but agreement of the numerical model results with test data is nonetheless still good as shown in these same references. Therefore, over a wide range of operating conditions of interest, the Boussinesq approximation is valid for the braking system application.

Depending on the Rayleigh number and geometric conditions, turbulent flow and heat transfer can be encountered during the brake cool down period. Direct numerical simulation (DNS) of turbulent natural convection using Eqs. (1)–(3) requires an extremely large number of grids to resolve the small scale flow features and, consequently, an extremely large core memory size and CPU time. This approach is impractical for the aircraft brake cooling problem which is three-dimensional, includes calculations in an extended computational domain, and requires reasonable computational efficiency in order to investigate design changes for enhanced cooling performance. Accurate calculation of the turbulent natural convection for engineering purposes can be made using turbulence models, however. In previous studies of the braking system subdomains as well as the current analysis of the wheel and brake assembly flow field, the $k-\varepsilon$ turbulence model has been employed. In this case, the governing equations are the time-averaged Reynolds equations of fluid motion and heat transfer along with the equations for kinetic energy k and dissipation of kinetic energy ε. These equations can be written in accordance with the previously stated assumptions as

Continuity.

$$\nabla \cdot \bar{\mathbf{u}} = 0 \tag{4}$$

Momentum.

$$\rho\left(\frac{\partial \bar{\mathbf{u}}}{\partial t} + \bar{\mathbf{u}} \cdot \nabla \bar{\mathbf{u}}\right) = -\nabla \bar{p} - \rho \mathbf{g} \beta (\bar{T} - T_\infty) + \nabla \cdot \tau_{\text{eff}} \tag{5}$$

Energy.

$$\rho c_p\left(\frac{\partial \bar{T}}{\partial t} + \bar{\mathbf{u}} \cdot \nabla \bar{T}\right) = \nabla \cdot (\lambda_{\text{eff}} \nabla \bar{T}) \tag{6}$$

Kinetic Energy.

$$\rho\left(\frac{\partial k}{\partial t}+\bar{\mathbf{u}}\cdot\nabla k\right)$$

$$=\nabla\cdot\left(\frac{\mu_t}{\sigma_k}\nabla k\right)+\frac{\mu_t}{\mathrm{Pr}_t}\mathbf{g}\beta\nabla\bar{T}+\mu_t\Phi-\rho\varepsilon \quad (7)$$

Dissipation.

$$\rho\left(\frac{\partial \varepsilon}{\partial t}+\bar{\mathbf{u}}\cdot\nabla \varepsilon\right)=\nabla\cdot\left(\frac{\mu_t}{\sigma_\varepsilon}\nabla \varepsilon\right)$$

$$+c_1(1-c_3)\frac{\varepsilon}{k}\frac{\mu_t}{\mathrm{Pr}_t}\mathbf{g}\beta\nabla\bar{T}+c_1\frac{\varepsilon}{k}\mu_t\Phi-\rho c_2\frac{\varepsilon^2}{k} \quad (8)$$

The standard $k-\varepsilon$ method used to model flow in the high Reynolds number core region cannot be used to model the effects of viscosity on the turbulence field in the viscous sublayer, and therefore an auxiliary treatment of the near-wall region is needed. A number of approaches to near-wall modeling including the law-of-the-wall technique, use of a one equation model near the wall and a two equation model away from it, and a low Reynolds number variant of the $k-\varepsilon$ turbulence model have been developed. The latter two methods may be more accurate than the law-of-the-wall technique, but require a very fine mesh to accurately resolve the sharp gradients of the flow variables in the near-wall region, which can lead to excessive computational cost. A near-wall modeling methodology that was applied to forced flows involving strong and subtle flow reversal by Haroutunian and Engelman (1991) and found to be more accurate than the $k-\varepsilon$ model using standard wall functions is employed in the present study. In this scheme, the mean flow equations are solved throughout the computational domain. The $k-\varepsilon$ model, however, is applied only up to and excluding a single layer of specialized elements located between the physical boundary and the fully turbulent outer flow field. In order to accurately resolve the local flow profiles, these wall elements employ specialized interpolation functions which are based on universal near-wall profiles and are functions of the characteristic turbulence Reynolds number. The turbulent diffusivity in the near-wall region is calculated using Van Driest's mixing length approach.

To more accurately calculate the temperature distributions within the thermally conductive wheel and brake components, the conjugate heat transfer problem is solved. Depending on whether the flow is laminar or turbulent, either Eqs. (1)–(3) or Eqs. (4)–(8), respectively, are solved in conjunction with the energy equation in the solid components, which is

$$\rho_w c_{pw}\frac{\partial T}{\partial t}=\nabla\cdot(\lambda_w\nabla T). \quad (9)$$

The temperature in Eq. (9) represents the temperature in the solid components, while the temperature in Eqs. (2), (3), and (5)–(8) is that of the fluid.

In the present study of turbulent natural convection within the wheel and brake assembly, the following nondimensional form of Eqs. (4)–(9) was employed (for brevity, the overbars indicating averaged values and the asterisks denoting the nondimensional quantities will be dropped, except for Ra^*_{ro}, from here on)

Fluid.

Continuity.

$$\nabla\cdot\mathbf{u}=0 \quad (10)$$

Momentum.

$$\sqrt{\frac{\mathrm{Ra}^*_{ro}}{\mathrm{Pr}}}\left(\frac{\partial \mathbf{u}}{\partial t}+\mathbf{u}\cdot\nabla\mathbf{u}\right)=-\nabla p-\sqrt{\frac{\mathrm{Ra}^*_{ro}}{\mathrm{Pr}}}\mathbf{e}T+\nabla\cdot\tau_{\mathrm{eff}} \quad (11)$$

Energy.

$$\sqrt{\mathrm{Ra}^*_{ro}\,\mathrm{Pr}}\left(\frac{\partial T}{\partial t}+\mathbf{u}\cdot\nabla T\right)=\nabla\cdot(\lambda_{\mathrm{eff}}\nabla T) \quad (12)$$

Kinetic Energy.

$$\sqrt{\frac{\mathrm{Ra}^*_{ro}}{\mathrm{Pr}}}\left(\frac{\partial k}{\partial t}+\mathbf{u}\cdot\nabla k\right)$$

$$=\nabla\cdot\left(\frac{\mu_t}{\sigma_k}\nabla k\right)+\frac{\mu_t}{\mathrm{Pr}_t}\mathbf{e}\nabla T+\mu_t\Phi-\sqrt{\frac{\mathrm{Ra}^*_{ro}}{\mathrm{Pr}}}\varepsilon \quad (13)$$

Dissipation.

$$\sqrt{\frac{\mathrm{Ra}^*_{ro}}{\mathrm{Pr}}}\left(\frac{\partial \varepsilon}{\partial t}+\mathbf{u}\cdot\nabla\varepsilon\right)=\nabla\cdot\left(\frac{\mu_t}{\sigma_\varepsilon}\nabla\varepsilon\right)$$

$$+c_1(1-c_3)\frac{\varepsilon}{k}\frac{\mu_t}{\mathrm{Pr}_t}\mathbf{e}\nabla T+c_1\frac{\varepsilon}{k}\mu_t\Phi-c_2\sqrt{\frac{\mathrm{Ra}^*_{ro}}{\mathrm{Pr}}}\frac{\varepsilon^2}{k} \quad (14)$$

Solid.

Conduction.

$$\sqrt{\mathrm{Ra}^*_{ro}\,\mathrm{Pr}}\left(\frac{\rho_w c_{pw}}{\rho c_p}\right)\frac{\partial T}{\partial t}=\left(\frac{\lambda_w}{\lambda}\right)\nabla^2 T \quad (15)$$

The nondimensional variables in the above equations are based on the following transformations:

$$r^*=\frac{r}{r_o},\quad z^*=\frac{z}{r_o},\quad u_i^*=\frac{u_i}{U},\quad t^*=\frac{tU}{r_o},\quad T^*=\frac{T-T_\infty}{(qr_o/\lambda)},$$

$$p^*=\frac{pr_o}{\mu U},\quad k^*=\frac{k}{U^2},\quad \varepsilon^*=\frac{\varepsilon}{(U^3/r_o)},\quad \Phi^*=\frac{\Phi}{(U^2/r_o^2)}$$

where the characteristic velocity of the flow is $U=(\alpha/r_o)\sqrt{\mathrm{Ra}^*_{ro}\,\mathrm{Pr}}$. Furthermore, the nondimensional turbulent and effective viscosities and turbulent and effective conductivities are

$$\mu_t^*=c_\mu\left(\frac{k^{*2}}{\varepsilon^*}\right)\sqrt{\frac{\mathrm{Ra}^*_{ro}}{\mathrm{Pr}}},\quad \mu^*_{\mathrm{eff}}=1+\mu_t^*$$

$$\lambda_t^*=\left(\frac{\mu_t^*}{\mathrm{Pr}_t}\right)\mathrm{Pr},\quad \lambda^*_{\mathrm{eff}}=1+\lambda_t^*.$$

The empirical constants in the above equations are taken as $c_1=1.44$, $c_2=1.92$, $c_3=1.44$, $c_\mu=0.09$, $\sigma_k=1.0$, $\sigma_\varepsilon=1.3$, and $\mathrm{Pr}_t=1.0$. Except for c_3, these constants are well established from experimental data for turbulent forced convection flows. Sensitivity studies were conducted to determine the effects of c_3 on the calculated results. It was found that there was very little variation in the heat transfer results and flow variables for a significant variation in c_3.

In Eqs. (11)–(15), the modified Rayleigh number Ra^*_{ro} is defined as

$$\mathrm{Ra}^*_{ro}=\frac{g\beta q r_o^4}{\lambda\alpha\nu}. \quad (16)$$

In previous studies of natural convection within closed and open-ended horizontal annuli involving a prescribed inner cylinder temperature T_i, Rayleigh numbers of the following form have been employed:

$$\mathrm{Ra} = \frac{g\beta(T_i - T_{\mathrm{ref}})l_c^3}{\alpha\nu}. \quad (17)$$

The Rayleigh number Ra referred to in later sections of this paper is based on the Eq. (17) definition, with characteristic length l_c corresponding to the annular gap width $r_o - r_i$. The Rayleigh numbers Ra_{ro} and Ra_{ri} found in later sections are also based on Eq. (17), but with l_c corresponding to the outer cylinder radius r_o and inner cylinder radius r_i, respectively.

Boundary Conditions

Solid Walls. At all stationary and impermeable boundaries of the fluid computational domain, the three components of velocity are set to zero to satisfy the no-slip condition

$$u_r = u_\theta = u_z = 0. \quad (18)$$

In studies of closed or open annulus natural convection where the fundamental aspects of the flow and heat transfer are of primary interest, the various solid boundaries are either set to a uniform temperature, subject to a uniform heat flux, or defined to be insulated. These basic thermal boundary conditions are specified as follows:

$$T = T_w \quad \text{(uniform temperature surface)} \quad (19)$$

$$-\lambda \frac{\partial T}{\partial n} = q \quad \text{(uniform heat flux surface)} \quad (20)$$

$$\frac{\partial T}{\partial n} = 0 \quad \text{(adiabatic surface)} \quad (21)$$

where n is the direction normal to the surface.

In a conjugate analysis of a braking system subdomain or of the overall wheel and brake assembly flow field, appropriate values of heat flux are usually applied to the wheel and brake solid components. These are intended to represent the heating of these components resulting either directly from frictional conversion of kinetic energy to thermal energy within the brake stack, or indirectly from conduction and radiation heat transfer to the wheel from the brake stack. The heat flux condition is written as

$$-\lambda_w \frac{\partial T}{\partial n} = q. \quad (22)$$

In the conjugate model, the following conditions are always satisfied at the interfaces of the solid components and the fluid:

$$T|_w = T|_f, \quad \left(\frac{\lambda_w}{\lambda}\right) \frac{\partial T}{\partial n}\bigg|_w = \frac{\partial T}{\partial n}\bigg|_f. \quad (23)$$

In the turbulent modeling approach previously described, the equations for k and ε are not solved in the specialized wall elements immediately adjacent to each impermeable wall. Therefore, the boundary conditions for these variables are applied at the first grid point away from the wall as prescribed by Eq. (24),

$$\frac{\partial k}{\partial n} = 0, \quad \varepsilon = \frac{(c_\mu k)^{1.5}}{\kappa\delta}. \quad (24)$$

Symmetry Planes. In cases where the natural convection flow and temperatures fields are symmetric about the vertical plane passing through the axis of the cylinders, the computational domain can be restricted to one side of this plane. The symmetry boundary condition applied at this plane requires that the component of velocity in the θ-direction and gradients of the remaining variables in the θ-direction are zero there. This assumption was justified in the present study based on the symmetry of the experimental results as well as comparisons with the results of simulations covering the entire domain. The boundary conditions at the angular symmetry plane are expressed as

$$\frac{\partial u_r}{\partial \theta} = u_\theta = \frac{\partial u_z}{\partial \theta} = \frac{\partial T}{\partial \theta} = \frac{\partial k}{\partial \theta} = \frac{\partial \varepsilon}{\partial \theta} = 0 \quad \text{at} \quad \theta = 0, \pi. \quad (25)$$

For the narrow gap brake stack/wheel subdomain modeled as shown in Fig. 4, the flow and temperature fields are assumed to be symmetric about the midaxial vertical plane. Therefore, the annulus and extended computational domain on one side of this plane is considered. The validity of this assumption has been confirmed in previous experimental studies of narrow gap open annuli such as that by Vafai et al. (1997). For the brake stack/wheel subdomain, the boundary conditions at the midaxial symmetry plane are

$$\frac{\partial u_r}{\partial z} = \frac{\partial u_\theta}{\partial z} = u_z = \frac{\partial T}{\partial z} = \frac{\partial k}{\partial z} = \frac{\partial \varepsilon}{\partial z} = 0 \quad \text{at} \quad z = 0. \quad (26)$$

Far Field. An extended computational domain is employed to overcome the difficulty in specifying boundary conditions at the open ends of the annular region without overconstraining the problem. This approach permits investigation of the complex interactions occurring between the fluid internal to the annulus and the external fluid in the vicinity of the open end. The issues involved in using an extended domain are addressed in more detail later on.

There are two pertinent choices for the far-field boundary conditions that can be used in an implicit numerical scheme which simultaneously incorporates the boundary and internal points into the solution algorithm at each time step. These are (Vafai and Ettefagh, 1990b)

$$\xi = 0, \quad T = T_\infty \quad \text{(Dirichlet)}$$

$$\frac{\partial \xi}{\partial n} = 0, \quad \frac{\partial T}{\partial n} = 0 \quad \text{(Neumann)}$$

where ξ in the above expressions represents either u_r, u_θ, u_z, k, or ε. Utilizing all Dirichlet conditions is physically valid only for very large extensions of the outer boundaries, which results in a substantial number of grid points and correspondingly large computational requirements. In previous open annulus and aircraft braking system subdomain studies, either all Neumann-type far-field boundary conditions or a combination of Dirichlet and Neumann conditions have been employed. The latter approach was adopted in the present study of the wheel and brake assembly flow field. Through numerical experimentation, it was determined that this provides a good approximation of the far-field conditions without an excessively large computational domain and without sacrificing the accuracy of the solution within the internal flow region or the near outer flow field. The size of the extended domain in the present study was set such that further extensions in the radial and axial directions produced negligible change in the results. The far-field boundary conditions used in the present study of the wheel and brake assembly flow domain, which is shown schematically in Fig. 5, are as follows:

$$\frac{\partial u_r}{\partial r} = \frac{\partial u_\theta}{\partial r} = u_z = \frac{\partial T}{\partial r} = \frac{\partial k}{\partial r} = \frac{\partial \varepsilon}{\partial r} = 0 \quad \text{at} \quad r = r_e \quad (27)$$

$$u_r = u_\theta = \frac{\partial u_z}{\partial z} = \frac{\partial k}{\partial z} = \frac{\partial \varepsilon}{\partial z} = 0,$$

$$T = T_\infty \quad \text{at} \quad z = l_1 + l_e \quad \text{and} \quad z = -l_2 - l_3 - l_e. \quad (28)$$

Fundamental Advancements

In this section, three categories of research which together provide a theoretical foundation for the study of buoyancy-induced cooling of an aircraft braking system are reviewed. The results of published studies of three-dimensional natural convection in cylindrical annuli with closed ends are discussed first. Comparison of this information with the results for open-ended annuli and braking system subdomains reviewed later underscores the substantial changes in the flow field and temperature distribution brought about by removing the impermeable end walls and thereby allowing the internal fluid to communicate with the ambient domain. It is also seen that the two cases are similar in some respects, provided certain conditions are met. A discussion of selected investigations of natural convection in a basic open rectangular cavity and several important aspects of this problem that are pertinent to convection within an open annulus is presented afterwards. It has been shown that the physical processes associated with interaction of the fluid internal to the cavity with the external flow field are very similar for the open rectangular cavity and open annulus geometries. Finally, the existing research work pertaining to three-dimensional buoyancy-induced flow and heat transfer within open cylindrical annuli, which is more closely representative of that within an actual aircraft braking system, is reviewed. The overview of fundamental research activity in this section, together with a review of studies more specifically related to three-dimensional flow and heat transfer within the wheel outboard, brake stack/wheel, and combined inboard and outboard flow domains presented later, is intended to provide a comprehensive framework for understanding and analyzing natural convection cooling of an aircraft braking system.

Closed Cylindrical Annuli. Buoyancy-induced flow and heat transfer in the annular space between concentric cylinders has been of interest to many researchers due to its many technological applications such as nuclear reactors, inert gas insulated electrical cables, solar receivers, thermal storage systems and, recently, aircraft brakes. Depending on the Rayleigh number and outer to inner cylinder radius ratio R, various types of laminar flow structures can arise in the core region of a sufficiently long horizontal annulus containing air. These structures were identified in some of the earlier experimental treatments of the problem. Liu et al. (1961) performed experiments using a heated inner cylinder and cooled outer cylinder to determine overall heat transfer correlations for R within the range of 1.15 to 7.5 using air, water, and silicone oil. For $R = 1.15$ with air and using tobacco smoke for visualization of flow patterns, they qualitatively described the transition from unicellular crescent shaped flow to a multicellular pattern in the top portion of the annulus as Rayleigh number was increased beyond a critical value. With further increase in Rayleigh number, the angular extent of the counter-rotating cells in the multicellular pattern increased and they began to oscillate slowly about the vertical. It was concluded that the upper region of a narrow gap annulus behaves like a "fluid heated from below" between horizontal plates, with Bénard type instabilities occurring at Rayleigh numbers in the range of Ra = 1600 to 2000.

A photographic study of annulus flow patterns was conducted by Bishop and Carley (1966) using air as the fluid medium. Uniform inner cylinder temperature was achieved by a vapor condensing method and flow visualization in the annular space was accomplished by transverse illumination after introduction of tobacco smoke. Two types of stable unicellular flow patterns were observed: the crescent eddy pattern for R up to 2.45, and the kidney shaped pattern for the largest R studied of 3.69. The period and amplitude of flow oscillations observed for $R = 3.69$ at higher Rayleigh numbers were reported. In experiments conducted by Grigull and Hauf (1966), a Mach-Zehnder interferometer and cigarette smoke were used for visualization of temperature and flow fields, respectively, in air. Their results revealed the existence of a three-dimensional spiral flow in the upper portion of the annulus for moderate R and increased Rayleigh number. Powe, et al. (1969) conducted experiments using an apparatus similar to that of Bishop and Carley (1966). Based on their results and those of previous investigators, they showed the existence of four laminar convective regimes in a closed horizontal annulus containing air: a *unicellular steady* regime for small Rayleigh number and any value of R, a *multicellular* regime for higher Rayleigh numbers and $R < 1.24$ (small gap annulus), a *spiral flow* regime for higher Rayleigh numbers and R between 1.24 and 1.71 (moderate gap annulus), and an *oscillating* regime for high Rayleigh number and $R > 1.71$ (large gap annulus). In a later numerical and experimental study by Kuehn and Goldstein (1976) the development of steady unicellular recirculating flow patterns in the core region of a large gap annulus, starting at low Rayleigh numbers where heat transfer occurs primarily by conduction and progressing to higher Rayleigh numbers where thin boundary layers are present on the inner and outer cylinders, was described for air. It was found that the center of rotation of the flow moves upward in the annulus with increased Rayleigh number.

The numerical studies of laminar natural convection between concentric cylinders have mainly concentrated on two-dimensional flow in the core region of long annuli and, to a much lesser extent, three-dimensional flow in shorter annuli with closed ends. A three-dimensional analysis is required for an annulus with finite axial length since the viscous shearing effect of the end walls affects the convection in the axial direction. Certain types of secondary flows which arise due to thermal instability, such as spiral flow in a moderate gap annulus, also require a three-dimensional analysis. Ozoe et al. (1979) conducted a numerical and experimental investigation of a vertically oriented annulus heated on the bottom end wall and cooled on the top wall. Their results showed that the stable flow consists of identical roll cells with axes oriented along radial lines within a single horizontal plane. The number of cells in the annulus was equal to the even integer nearest to the average circumference divided by the height. The effects of annulus inclination for the same problem were later investigated numerically and experimentally by Ozoe et al. (1981). The three-dimensional governing equations were formulated in terms of vorticity and vector potential and solved by the finite difference method. Numerical calculations were performed for Prandtl number of 10. They reported that, as the heated surface is inclined from the lower horizontal position, the mean Nusselt number at first decreases as the circulation pattern changes from a symmetrical array of roll cells to distorted and oblique roll cells to a single circulation. With further inclination, the mean Nusselt number increases until going through a maximum and then decreases to unity as the heated surface reaches the upper horizontal position.

Takata et al. (1984) numerically and experimentally studied the effects of inclining a large-gap closed annulus having a heated inner cylinder and cooled outer cylinder for a fluid with Prandtl number of 5000. The vorticity-vector potential form of the three-dimensional governing equations was solved using the SOR procedure. Flow visualization was accomplished using glycerol as the working fluid and suspended aluminum powder as a seeding material. The results of this investigation indicated that a co-axial double helix flow pattern is present adjacent to each end wall inside the horizontal annulus. For the horizontal orientation, the flow has a relatively small component of axial velocity. When the annulus is tilted, the axial velocity increases considerably and a more distorted co-axial double helix is present. It was found that while the maximum local Nusselt numbers show a strong dependence on the inclination angle, the average Nusselt number increases only slightly as the inclination increases. Three-dimensional numerical simulations of natural convection in a moderate gap horizontal annulus were conducted by Rao et al. (1985), also for a fluid with Prandtl number of 5000. They found that a spiral-type flow was present in the upper portion of the annulus in conjunction with nearly two dimensional flow in the lower regions. The structure of the flow pattern was confirmed by an experimental visualization study using glycerol as the working fluid. It was seen from the experimental and numerical results that for this high Prandtl number the number of spiral vortices tends to increase as Rayleigh number is increased.

A three-dimensional numerical study of natural convection in a large-gap closed horizontal annulus filled with air was performed by Fusegi and Farouk (1986) using the vorticity-velocity formulation. The length of the annulus was chosen to be small so that the influence of the end walls was evident in the fluid motion. Double helical roll structures qualitatively similar to that reported by Takata et al. (1984) were calculated. Transient three-dimensional buoyancy-driven flow and heat transfer in a large-gap closed horizontal annulus was numerically investigated by Vafai and Ettefagh (1991a). Calculations were performed for a Prandtl number corresponding to that of air, and therefore the results are of greater practical applicability than previous studies at much higher Prandtl numbers. The results showed that a core region in which the temperature distribution remains unchanged and the flow is essentially two-dimensional is present at the mid-axis of the annulus, provided the length to outer radius ratio is adequately large. The effects of the axial impermeable boundaries were shown to be characterized by retardation of the flow field through the viscous shearing force in regions near the end walls. Accordingly, the local Nusselt number experiences a reduction at the end walls. The transient development of the flow and temperature fields as a result of sudden heating of the inner cylinder was presented.

A numerical and experimental investigation of the development of three-dimensional buoyancy-induced flow and temperature fields in moderate and large-gap closed horizontal annuli was conducted by Dyko et al. (1999). It was shown that in a moderate gap annulus, the natural convective flow at low Rayleigh numbers is similar to that in a large gap annulus, with crescent-shaped flow patterns (r-θ plane) in the core region and a rotating cell (r-z plane) located in the upper portion of the annulus at each end wall. As Rayleigh number is increased above a critical value, however, an integral number of transverse spiral vortex pairs forms between the end vortices in the moderate gap annulus due to thermal instability. The size of the inner vortical cells was shown to depend on the natural size predicted by stability theory for an infinitely long annulus, the increase in Rayleigh number above the critical value, and the length of the annulus. The Nusselt number distribution in the upper part of the annulus was found to be significantly influenced by the vortex structures. The results of the investigation by Dyko et al. (1999) showed that in a sufficiently long large-gap annulus, three stable flow regions coexist at higher Rayleigh numbers. First, a three-dimensional recirculating flow consisting of a transverse vortex in the upper portion of the annulus and a double helical flow structure below this sets up next to each end wall. In the core region, the thermal field retains the characteristics of that associated with two-dimensional flow. Finally, between the end wall and core zones a third region is present in which the primary flow circulation takes place in the axial planes in conjunction with much lower speed axial flow. For a large-gap annulus filled with a high Prandtl number fluid, it was shown that the crescent-shaped flow patterns present at low Rayleigh numbers change to symmetric unicellular structures with centers of rotation near the top of the annulus as Rayleigh number is increased. Longitudinal roll cells are positioned at the top of the annulus for the larger Rayleigh number flows. The numerical results presented by Dyko et al. (1999) were shown to be in excellent agreement with the experimental results for both Prandtl numbers studied.

A numerical study of the effects of an inner cylinder geometric perturbation on three-dimensional natural convection in a closed horizontal annulus was performed by Iyer and Vafai (1997). The fundamental structure of the flow field and the heat transfer characteristics associated with this geometry were analyzed and compared with that of the regular annulus without any perturbation. The effect of variation of a number of key geometric parameters of the perturbation on the overall heat transfer was also presented. Iyer and Vafai (1998) also conducted a detailed study of buoyancy-induced flow and heat transfer in a closed horizontal annulus having multiple geometric perturbations on the inner cylinder. The flow field structures corresponding to different numbers of perturbations and pertinent geometric variations were analyzed, and heat transfer effects were studied by analyzing local and average Nusselt numbers. As was the case for the single perturbation, the flow field was found to evolve from the entrainment of flow by the heated vertical portion of the perturbation. As more perturbations were added, the flow field changed in a regular and recurring manner. Qualitative similarities in the local Nusselt number distributions for different numbers of perturbations were also observed. The results showed that the overall heat transfer rate increases substantially with introduction of multiple perturbations of the size considered.

The number of experimental and numerical studies of buoyancy-induced turbulent flow in annular geometries, which is pertinent to aircraft brakes due to the high Rayleigh numbers that are attained, is very limited. Kuehn and Goldstein (1978) conducted an experimental study of the influence of Rayleigh number and eccentricity on natural convection between two horizontal isothermal cylinders. Results for the concentric cylinder case using nitrogen showed that the flow first becomes unsteady in the plume above the inner cylinder, and that with further increases in Rayleigh number this becomes turbulent. The turbulence in the plume is transported to the top of the outer cylinder and decays as the flow proceeds downward along the outer cylinder to the lower half of the annulus. The flow in the bottom half of the annulus remains laminar and is virtually steady. The transition to turbulent flow in the annulus of $R = 2.6$ that was studied occurred for $\mathrm{Ra} > 10^6$. An experimental study of turbulent natural convection of helium between horizontal concentric cylinders maintained at cryogenic temperatures was conducted by Bishop (1988). Time-averaged temperature profiles and overall heat transfer rates were obtained for Rayleigh numbers in the range of $\mathrm{Ra} = 6 \times 10^6$ to 2×10^9 and expansion numbers ($\beta\Delta T$) from 0.20 to 1.0. The study was conducted for an annulus with a radius ratio of $R = 3.36$. The heat transfer rate was found to be dependent on both the expansion number and the Rayleigh number. Using the same basic test apparatus and fluid but with an annulus of $R = 4.85$, McLeod and Bishop (1989) presented time-dependent temperature data and discussed the spatial extent of turbulence in the annulus as well as the postulated flow structures based on these measurements. In these experiments, the inner and outer cylinders were maintained at cryogenic temperatures. It was determined that increasing the expansion number from 0.25 to 1.0 results in a more turbulent flow structure and increased heat transfer, which further substantiated the conclusion of Bishop (1988) that the expansion number, in addition to Rayleigh number, should be accounted for in calculating the heat transfer rate.

A numerical study of turbulent natural convection in a large-gap annular geometry was conducted by Farouk and Guceri (1982). They carried out two-dimensional simulations over the Rayleigh number range of $\mathrm{Ra} = 10^6$ to 10^7 using the $k-\varepsilon$ turbulence model. The differential equations for time-averaged vorticity, stream function, temperature, turbulent kinetic energy, and dissipation rate of turbulent kinetic energy were solved using a finite difference technique. The results were found to be in good agreement with the available experimental data in the literature. The direct numerical simulation (DNS) of three-dimensional turbulent flow within closed annuli, which is a taxing computational task owing to the fine mesh resolution and time step size necessary to capture the details of the small scale eddies, has recently become more practical due to the development of supercomputers. Morita et al. (1990) demonstrated the applicability of DNS to the problem of three-dimensional, unsteady, turbulent natural convection in an annulus. Fukuda et al. (1990) carried out the DNS for a large-gap annulus using the explicit leap-frog scheme and the approximation of periodic boundary conditions in the axial direction. Analyses were conducted for Rayleigh numbers up to $Ra = 6 \times 10^5$. The results were verified by comparison with experimentally obtained time averaged velocity and temperature profiles and turbulence quantities such as intensities of velocity and temperature fluctuations. The DNS captured the general trend of the stable flow pattern changing to a periodic and then irregular turbulent flow. Three-dimensional DNS and LES (large eddy simulation) of turbulent flow was performed for Rayleigh numbers up to $Ra = 1.18 \times 10^9$ by Fukuda et al. (1991) using the explicit finite difference method. Their results were found to be in good agreement with experimental data from other investigators.

Turbulent natural convection in a horizontal annulus was numerically investigated for a wide range of parameters ($10^6 < Ra < 10^9$, $0.01 < Pr < 5000$, $1.5 < R < 11$) by Desai and Vafai (1994). Discretization of the time averaged governing equations was achieved using a finite element method based on the Galerkin method of weighted residuals, and the $k-\varepsilon$ turbulence model was applied. A comprehensive analysis was presented for the effects of varying Rayleigh number and Prandtl number on the time-averaged flow and temperature fields and Nusselt numbers, as well as the effect of R on isotherms and Nusselt numbers. The heat transfer rates were found to be substantially higher than those for laminar flow. The heat transfer decreased with an increase in R for the same Rayleigh number. As Prandtl number was increased, the turbulent viscosity decreased indicating lower levels of turbulence at the same Rayleigh number. The mean cavity Nusselt number increased with higher Prandtl number up to $Pr = 100$ for $Ra = 10^8$ and $R = 2.6$. Transition to turbulence was delayed for fluids with Prandtl numbers of 1000 and 5000, however, which resulted in lower heat transfer at the same Rayleigh number since the flow was still in the laminar regime. Desai and Vafai (1994) also provided results from a three-dimensional model to show the influence of the end walls on the natural convection. The local Nusselt number experienced a drastic decrease at the end walls. As in the laminar case studied by Vafai and Ettefagh (1991a), it was shown that if the annulus is sufficiently long, there exists a core region over a substantial length of the annulus in which a two-dimensional approximation can be made. Good agreement between results from this investigation and those of previous experimental and numerical studies was shown.

Open Rectangular Cavities. Natural convection in open-ended structures has been an active area of research in recent years, with most of the studies dealing numerically with two-dimensional open rectangular cavities. The interest in this problem stems from applications such as cooling of electronic equipment, energy conservation in buildings, fire research, and solar receiver systems. The open rectangular cavity studies have provided valuable insight into the coupling of the internal and external flow fields and have served as a stepping stone toward the more recent treatment of the open annulus. Investigations have been conducted to ascertain the effects of parameters such as Rayleigh number (Le Quere et al., 1981; Penot, 1982; Chan and Tien, 1983, 1985a, b, 1986; Humphrey and To, 1986; Vafai and Ettefagh, 1990a; Skok et al., 1991; Mohamad, 1995), Prandtl number (Bejan and Kimura, 1981; Vafai and Ettefagh, 1990a), cavity aspect ratio (Le Quere et al., 1981; Humphrey and To, 1986; Vafai and Ettefagh, 1990a; Mohamad, 1995), and cavity inclination (Le Quere et al., 1981; Penot, 1982; Humphrey and To, 1986; Mohamad, 1995) on the open rectangular cavity flow and thermal fields and heat transfer. The effects of partially obstructing the opening have also been examined (Hess and Henze, 1984; Abib and Jaluria, 1988; Miyamoto et al., 1989). Various types of thermal boundary conditions such as all walls heated or only the back wall heated have been employed. Although these conditions affect the local flow and temperature fields, they do not substantially alter the basic flow mechanisms, which have been identified by Vafai and Ettefagh (1990a). Additional features of the outer and inner domain interactions are discussed in Ettefagh and Vafai (1988) and Ettefagh et al. (1991). An examination of the literature pertaining to open rectangular cavities is of interest in the present work because several key aspects of thermally driven flow in open rectangular cavities are also of importance in the open annulus case as related to the wheel outboard, brake stack/wheel, and wheel and brake assembly configurations.

One of the main difficulties encountered in the analysis of buoyancy-driven flow in open cavities is the specification of appropriate boundary conditions at the open ends, where physical conditions are unknown. In the numerical investigation by Le Quere et al. (1981) of an open rectangular cavity with uniform temperature walls, this was overcome by utilizing a short extended computational domain. Numerical tests were performed in which the position of the extended boundaries and the conditions set at these locations were varied. They stated that the flow and heat transfer inside the cavity were not affected by these conditions if the boundary of the extended domain is positioned two cavity heights or more from the aperture plane. It should be noted that in later studies by Vafai and Ettefagh (1990a, b) of a rectangular cavity open on both ends, it was determined that a much larger extension is required for the results inside the cavity not to be affected by the far-field conditions. Using the finite difference method, Le Quere et al. (1981) performed simulations over a range of Grashof numbers (based on the aperture plane dimension) from 10^4 to 3×10^7. For a cavity of aspect ratio $a/c = 1$ with Grashof number of 10^5, where a is the cavity width and c the cavity height, the flow was found to be steady and entered the cavity along the bottom $\frac{2}{3}$ of the aperture plane while exiting back to the ambient along the upper $\frac{1}{3}$ of this plane. For the conditions studied, flow recirculation did not arise in the cavity. At Grashof numbers exceeding 10^7, the flow became noticeably unsteady and localized recirculation zones formed along the bottom of the cavity. A periodic recirculating process in the top half of the aperture plane was also present.

Chan and Tien (1985b) compared two methods of addressing the problem of unknown physical conditions at the aperture plane: use of an extended computational domain and restriction of the computations to within the cavity. The motivation for the latter approach is savings of memory and computational time. In their numerical analysis of a square open cavity with heated back wall using the second approach, the temperatures of fluid entering the cavity were set to the ambient value and the temperatures of fluid exiting the cavity satisfied the upwind condition assuming conduction to be small relative to convection. The gradient of vertical velocity was set to zero at the opening and the horizontal velocity was determined by the continuity equation. With conditions at the cavity opening thus set, it was found that the isotherms were not predicted as accurately at lower Rayleigh numbers, which is when conduction is dominant. At higher Rayleigh numbers heat transfer was predicted fairly well, but certain flow characteristics such as the turn and separation around the lower corner were missed.

In a shallow cavity, the heat transfer rate and flow patterns are affected less by the manner the open boundaries are set because of the large distance between open and closed ends. Using the simplified approach of confining computations to within the cavity, Chan and Tien (1985b) performed numerical calculations for a shallow cavity heated at the back wall over the Rayleigh number range of 10^3 to 10^6. At lower Rayleigh numbers, they found that the effect of the open boundary does not penetrate very far into the cavity, and a core region exists in which the velocity field is everywhere parallel to the horizontal walls. As Rayleigh number is increased, the effects of the open boundary extend further into the cavity and the core region begins to disappear. A boundary layer forms at the vertical heated wall and the fluid heated by this wall accelerates at first gradually and then rapidly as it moves along the upper wall and exits the open end. Based on comparison of the numerical results with test data obtained by Chan and Tien (1983) using LDV and a thermocouple probe, it was concluded that the numerical model was adequate for predicting the basic flow patterns and heat transfer characteristics within a shallow open cavity. Both the numerical and experimental results showed that the flow remains ''unicellular'' throughout with no recirculation or secondary cell. The experimental results also showed that the exiting flow, which is driven by the heated cavity, was not strong enough to form a buoyant jet for Rayleigh numbers even as high as approximately 10^6 to 10^7. Instead, a wall plume rose up the vertical wall above the opening entraining fluid from the surroundings in the process. In the case where the fluid was thermally stratified the incoming flow approached horizontally, while in the case of no stratification it was expected to approach radially toward the lower part of the opening. It was therefore concluded that the incoming flow is significantly affected by the external conditions.

Buoyancy-induced convection in open-ended rectangular cavities was analyzed by Vafai and Ettefagh (1990a) for Rayleigh numbers in the range of 10^3 to 5×10^5. A thorough examination of the transient behavior of the flow and temperature fields and the effects of varying Rayleigh number, Prandtl number, temperature ratio between the upper and lower blocks, and cavity aspect ratio on the flow and temperature fields and heat transfer was presented in this study. It was determined that the size of the enlarged domain had to be at least 60 times the height of the cavity for higher Rayleigh numbers to eliminate the effects of the far-field solution on the flow field and heat transfer inside the cavity and near its opening, which is far greater than that anticipated by previous researchers. The results of this study showed that at lower Rayleigh numbers the heated fluid rises in a buoyant plume into the ambient domain as it leaves the cavity. As a result of this *ejection* mechanism, which is caused by energy transfer from the internal cavity surfaces to the fluid, the colder ambient fluid enters the cavity to replace the departing hot fluid. The departing fluid leaves at a higher velocity than the incoming fluid, and therefore it occupies a smaller portion of the aperture plane due to conservation of mass. As Rayleigh number is increased, the heated fluid exits at higher velocities due to greater buoyancy force and the colder fluid is sucked further into the cavity at higher speed. In the upper part of the cavity, the horizontal temperature gradient decreases with increasing Rayleigh number resulting in a thermally stratified region along the upper wall. While the ejection mechanism results in upward flow that is opposite the direction of the gravity field, the *suction* mechanism caused by the fluid filling the void left by the departing plume causes a parallel horizontal flow along the lower wall of the cavity. The horizontal flow along the lower wall experiences significant buoyancy forces. These two effects give rise to an instability mechanism described in detail by Vafai and Ettefagh (1990b). As Rayleigh number is increased more, the cold fluid penetrates even further into the cavity and a thermal boundary layer forms along the lower wall. In addition, the outgoing fluid rises up much faster resulting in a thinner thermal boundary layer along the wall outside the cavity. As a result of this thinner boundary layer, which is responsible for most of the heat transfer to the ambient fluid, the temperature of the plume decreases. At the highest Rayleigh number studied, a circulating flow region is formed inside the cavity due to the viscous interaction of the incoming and outgoing flows.

Open Cylindrical Annuli. Natural convection in horizontal cylindrical annuli open on one or both ends, which is representative of that which occurs in the actual aircraft braking system wheel outboard and brake stack/wheel regions, respectively, has only very recently been studied. While the open annulus geometry has some similarities to that of the closed annulus, there are some substantial differences in flow behavior due to axial transport effects induced by the open ends in conjunction with the buoyancy-driven flow in each axial plane of the cavity. Also, in contrast to the open rectangular cavity which can be analyzed using a two-dimensional model, the open annular cavity flows are strongly three-dimensional because of these effects and as such cannot even be approximated with a two-dimensional model. The first treatment of the open annular cavity problem was by Vafai and Ettefagh (1991b), who studied transient laminar natural convection in a horizontal annulus open on both ends with the inner cylinder heated and outer cylinder cooled. The ADI and extrapolated Jacobi schemes were employed to solve the vorticity-vector potential form of the time-dependent governing equations and an extended computational domain was utilized to properly account for the open boundaries. Calculations were performed for Rayleigh numbers of $Ra_{ro} = 4.3 \times 10^3$ and 10^4.

The results of this study showed that flow inside the open annulus is comprised of recirculation in each axial plane driven by the heated inner and cooled outer cylinders in conjunction with axial movement due to interaction of the internal fluid with the external fluid. Near the open ends, the strength of the recirculation decreases and the axial velocity increases. The isotherms are spaced much closer to the inner cylinder at the aperture plane and therefore the heat transfer from the inner cylinder is considerably enhanced there. The heat transfer over the upper part of the outer cylinder is also greater at the opening. The existence of a core region in which the temperature field can be approximated as two-dimensional for Rayleigh numbers less than $Ra_{ro} = 10^4$, provided the annulus is sufficiently long, was revealed. It was found that this approximation is not valid for the flow field, however, which is different from a closed annulus where both the flow and temperature fields are nearly two-dimensional in the core region as shown by Vafai and Ettefagh (1991a). In both the closed and open annulus studies, the extent of the core region was found to decrease with increased Rayleigh number. The transient development of the open annulus flow and temperature fields resulting from sudden heating of the inner cylinder was also investigated by Vafai and Ettefagh (1991b). It was observed that the errors for a two-dimensional assumption in the midportion of the annulus are less at earlier times during the transient development of the flow and temperature fields.

In another study, Ettefagh and Vafai (1991) showed that the strong coupling effects between the flow inside and outside the open annulus resulted in the three physical and fundamental transport mechanisms of *ejection, mixing,* and *suction,* which are similar to those in an open rectangular cavity. At the aperture plane, the recirculation pattern inside the annulus is no longer present and the heated fluid around the outer cylinder rises radially in the axial plane. Hot fluid exits the annulus at both the top of the outer cylinder and bottom of the inner cylinder due to the *ejection* mechanism, which is caused by energy transfer from the inner cylinder surface to the fluid. Cold fluid from the surroundings is drawn into the annulus at the top of the inner cylinder and bottom of the outer cylinder as a result of the *suction* mechanism caused by replacement of the fluid lost from the annulus. The velocity of fluid leaving the annulus at the top of the outer cylinder is significantly higher than that of fluid entering along the top of inner cylinder. However, fluid entering the annulus along the lower part of the outer cylinder is approximately at the same velocity as that exiting along the bottom of the inner cylinder. In the external region immediately adjacent to the aperture plane, *mixing* of the fluid departing from the annulus along the lower part of the inner cylinder with the cold fluid entering the annulus along the top of the inner cylinder occurs. This mixing mechanism has a direct influence in increasing the temperature of the surrounding fluid.

The results of the study by Ettefagh and Vafai (1991) also showed that at the lower Rayleigh number of $Ra_{ro} = 4.3 \times 10^3$, the magnitude of the inner cylinder local Nusselt number at the aperture plane is greater than its value at the core region by a factor of 2 at the top of the annulus and a factor of 3 at the bottom of the annulus. Also, at the top of the annulus the outer cylinder local Nusselt number at the aperture plane is 2.4 times greater than its value at the core region, while at the bottom of the annulus it is three times less than at the midaxial plane. Within ± 60 deg of the top of the annulus the outer cylinder local Nusselt number at the aperture plane is greater than at the core region, while below this region it is less than at the midaxis. An increase in Rayleigh number was shown to cause a sharp increase in the rate of heat transfer in the vicinity of the aperture plane.

Turbulent natural convection in a narrow-gap horizontal annulus open on both ends was recently investigated numerically and experimentally by Vafai et al. (1997). This study provided, for the first time, a description of the turbulent buoyancy-induced flow and a quantitative evaluation of the effects of varying geometric parameters on heat transfer in a narrow gap open annulus. As discussed later in the brake stack/wheel subdomain section of this paper, the results of this study revealed some of the basic differences between flow in a narrow-gap open annulus and that in a wider-gap open annulus. Natural convective air flow in the narrow open-ended annulus between a heated inner drum and cooled outer cylinder was studied experimentally by Braun et al. (1997). Visualization of the flow inside the annulus and mapping of the inner and outer cylinder temperature distributions was performed over a range of Rayleigh numbers in which the stable laminar flow transitions to a higher strength unstable laminar flow. An aluminum inner cylinder and Lucite outer enclosure were employed in the experiments. By filling the outer enclosure with an oil having the same refractive index as Lucite, an undistorted sheet of laser light could be introduced into the annulus to illuminate particles entrained in the natural convection currents. At the lower Rayleigh number studied of $Ra = 6.6 \times 10^3$, it was determined from photographic images of the flow patterns that the air enters the lower regions of the annulus and is drawn inward toward the midaxial plane. At the same time, portions of the flow proceed circumferentially upward. At the midaxial plane, the remaining air moves circumferentially into the upper region of the annulus and then reverses axial direction. At the higher Rayleigh number studied of $Ra = 1.6 \times 10^4$, the flow in the upper portion of the narrow gap annulus became unstable.

Braking System Subdomains

Wheel Outboard Region. As illustrated in Fig. 3, the wheel outboard subdomain is modeled as a wide-gap annulus of small axial length open to the ambient surroundings on one end and closed on the other. The outer cylinder, inner cylinder, and end wall of the annulus correspond to the wheel outboard flange, wheel hub, and wheel web, respectively. A numerical investigation of laminar natural convection for fundamental geometries of this type was performed by Desai and Vafai (1992) using the Galerkin method of finite element formulation. In this study, fundamental thermal boundary conditions consisting of a uniform temperature cold outer cylinder, uniform temperature hot inner cylinder, and an adiabatic end wall were employed. The effects of Rayleigh number and inner cylinder length were studied. Results of the investigation showed that at a Rayleigh number of $Ra_{ro} = 10^4$, the effect of the closed end wall is to retard the flow coming into the cavity through the aperture plane. At a Rayleigh number of $Ra_{ro} = 10^6$, the closed end wall causes the formation of two spirally rotating cells inside the cavity, separated by an axially stagnant flow region. At both the low and high Rayleigh numbers, there is a considerable enhancement in heat transfer in the vicinity of the open end. It was found that reducing the length of the inner cylinder causes higher heat transfer rates from the inner cylinder for both low and high Rayleigh number cases. This is a result of the higher velocities associated with the annular cavity having a shorter inner cylinder and the stagnant region occupying a smaller portion of the cavity which causes better interaction of the ambient fluid with the cavity fluid. The transient three-dimensional natural convection flow and heat transfer associated with this geometry was also investigated by Desai and Vafai (1993). The numerical results showed the evolution of the natural convection flow field in the annulus and its immediate surroundings resulting from sudden heating of the inner cylinder.

The annular cavity with one end open to the ambient surroundings has been studied experimentally and numerically by Desai and Vafai (1996) for high Rayleigh number conditions resulting in turbulent natural convection. This work provided, for the first time, validated heat transfer data for high Rayleigh number buoyancy-induced flows in open annular cavities. In the experimental portion of this investigation, a test section with aluminum inner and outer cylinders and an aluminum end wall was employed. A constant heat flux was applied to each of these components. Local surface temperature measurements were made to determine heat transfer characteristics of the convective flow. Nusselt number correlations were developed and presented for individual components of the cavity as well as the entire cavity over the Rayleigh number range of $Ra^*_{ro} = 1.27 \times 10^9$ to 5.05×10^9. These correlations are given in Eqs. (29)–(33)

$$Nu_{av} = 0.0136(Ra^*_{ro})^{0.376} \quad \text{(outer cylinder)} \tag{29}$$

$$Nu_{av} = 0.0133(Ra^*_{ro})^{0.379} \quad \text{(end wall)} \tag{30}$$

$$Nu_{av} = 0.0113(Ra^*_{ro})^{0.381} \quad \text{(inner cylinder)} \tag{31}$$

$$Nu_{av} = 0.0119(Ra^*_{ro})^{0.378} \quad \text{(inner cylinder tip)} \tag{32}$$

$$Nu_{av} = 0.0131(Ra^*_{ro})^{0.378} \quad \text{(cavity)}. \tag{33}$$

In the numerical part of the study, the $k-\varepsilon$ model was employed for simulating turbulent characteristics of the convective flow and the conjugate problem was solved to account for heat conduction in the walls of the cavity. Good agreement between the numerical and experimental results was shown. It was found that the fluid enters the lower half of the annular cavity axially due to the suction mechanism. Some of this fluid becomes entrained in the boundary layers on the inner and outer cylinders, while the remainder proceeds axially toward the cavity end wall and then rises in a boundary layer along this wall. In the upper part of the cavity, the fluid motion is characterized primarily by the rising plume from the top of the inner cylinder and the strong axial outflow of the heated fluid. The fluid is ejected from the top of the cavity as a buoyant jet. There is also a region of outflow immediately below the inner cylinder and inflow just above it.

In the study by Desai et al. (1996), the influence of various geometric parameters on the turbulent flow characteristics and heat transfer of the open annular cavity geometry was investigated numerically. Four different pertinent geometries were analyzed and thermal performance in terms of average surface temperature and Nusselt number were compared. The configurations studied can be classified as equally extended inner and outer cylinders, no outer cylinder, extended inner cylinder, and conical inner cylinder. The same total heat input was applied to each configuration in order to evaluate their relative thermal performance. It was found that changing the inner cylinder shape from cylindrical to conical improves the penetration of ambient air into the cavity and therefore improves the cooling characteristics. The average surface temperature of the configuration with a conical inner cylinder was approximately the same as the equally extended inner and outer cylinder design in spite of the reduced surface area. It was also shown that eliminating the outer cylinder results in the highest heat transfer rates from the cavity because of the improved interaction with the ambient air. However, the surface temperatures are highest because of the reduced surface area. The extended inner cylinder configuration resulted in the lowest surface temperatures, mainly because it had the greatest surface area.

Brake Stack/Wheel Region. The brake stack/wheel inboard subdomain is represented by a narrow gap annulus open at both ends to the ambient as shown in Fig. 4. The inner and outer cylinders correspond to the aircraft brake stack and wheel, respectively. An experimental and numerical study of turbulent buoyancy-induced flow in a narrow-gap open-ended annulus was performed for the first time by Vafai et al. (1997). A test section with aluminum inner and outer cylinders and aluminum vertical walls on either side of the inner cylinder was employed in the experiments. The aluminum end walls extended radially from $r = r_s$ to $r = r_i$ (Fig. 4). A constant heat flux was applied to the inner cylinder and vertical end walls using electrical heaters. Experiments were conducted over the range of Rayleigh numbers from $\mathrm{Ra}^*_{ro} = 7.09 \times 10^8$ to 4.76×10^9. Temperature distributions of the component surfaces resulting from the buoyancy-driven air flow occurring in the gap between the inner and outer cylinder and in the external region adjacent to the end walls were recorded. These were utilized for development of average Nusselt number relations, description of the thermal behavior, and validation of the numerical model, results of which compare very well with the experimental data. Smoke flow visualization using laser illumination was performed to illustrate flow patterns in the vicinity of the open ends. A Nusselt number correlation for the inner cylinder and its two vertical end walls which applies over the previously mentioned Rayleigh number range was developed and is given in Eq. (34)

$$\mathrm{Nu}_{av} = 0.134(\mathrm{Ra}^*_{ro})^{0.264}. \tag{34}$$

In the numerical part of the narrow-gap annulus study, the three-dimensional governing equations were discretized using a finite element formulation and the $k-\varepsilon$ model was utilized for simulation of the turbulent flow. From the conjugate numerical results and flow visualization experiments, the latter of which qualitatively confirmed pertinent features of the numerically calculated flow field, the structure of turbulent flow within the annulus was determined. It was shown that the bulk flow is characterized by suction of cold fluid into approximately the lower two-thirds of the aperture plane and ejection of hot fluid at the top as a high-speed buoyant jet. The maximum axial penetration of fluid entering the annulus is at the lowermost angular position and the penetration diminishes in the upward direction. The fluid pathlines in the axial planes of the annulus are concentric circles, indicating a flow pattern similar to that in a narrow channel. As the fluid rises to the top portion of the annulus it reverses axial direction and then leaves the annulus. Fluid rising along the vertical faces adjacent to the inner cylinder becomes entrained in this buoyant flow exiting from the top of the annulus.

From the results of this study, it is seen that there are some major differences in flow characteristics compared to the wheel outboard cavity turbulent flow field previously described. These include the occurrence of channel type flow between the inner and outer cylinders of the narrow annulus as opposed to the free surface type boundary layer flow present in the much wider annular gap of the wheel outboard region, and an absence of the buoyant plume rising from the inner cylinder which is a prominent feature of the wider gap cavity flow. In addition, there is no localized inflow of ambient air above the inner cylinder or outflow below the inner cylinder, which are present in the wider gap cavity. Although the flow behavior in a narrow gap annulus is markedly different in many respects from that in a large-gap open annular cavity, in both cases the interaction between the inner and outer flow fields has been shown to result in locally enhanced heat transfer near the open ends.

In order to identify geometric parameters of the narrow-gap open annulus that are important to improved cooling performance, the effects of variations in inner to outer cylinder annular gap width and inner cylinder length were investigated by Vafai et al. (1997). For the baseline case, an outer-to-inner cylinder radius ratio of $R = 1.1$ and an inner cylinder length-to-radius ratio of $L = 0.5$ were chosen. Two configurations having the baseline inner cylinder length but radius ratios of $R = 1.075$ and $R = 1.05$, respectively, and two configurations having the baseline radius ratio but length-to-radius ratios of $L = 0.375$ and $L = 0.25$, respectively, were also modeled. The studies were carried out up to a Rayleigh number of $\mathrm{Ra}_{ri} = 1 \times 10^6$. At any given Rayleigh number, it was found that the average inner cylinder Nusselt number decreases with a decrease in the gap size between the inner and outer cylinders. The average Nusselt number decreased by approximately 60 percent and 80 percent for radius ratios of $R = 1.075$ and $R = 1.05$, respectively, compared to baseline. For $L = 0.25$, the average Nusselt number was higher than that for the baseline case of $L = 0.5$ up to a Rayleigh number of about $\mathrm{Ra}_{ri} = 6 \times 10^5$, and was lower than baseline above this Rayleigh number. Similar behavior was calculated for $L = 0.375$, except the change in trends occurred at about $\mathrm{Ra}_{ri} = 2 \times 10^5$. It was thus found that at lower Rayleigh numbers reduced length results in greater interaction of the internal and external flows and increased Nusselt number. At higher Rayleigh numbers where the axial penetration of the higher velocity inflow is much greater, the increase in Nusselt number is caused by increased length which results in a higher heat transfer area. These results suggest that an optimum inner cylinder length exists for a given operating condition at which convection heat transfer can be maximized. Correlations for the inner cylinder Nusselt number as a function of Rayleigh number, inner cylinder length to radius ratio, and outer to inner cylinder radius ratio were developed and are provided in Eqs. (35) and (36).

$$\mathrm{Nu}_{av} = 0.2(\mathrm{Ra}_{ri})^{0.14}(1 - 0.705L)[1 + 27.74(R - 1)]: \quad \mathrm{Ra}_{ri} < 1 \times 10^5 \tag{35}$$

$$\mathrm{Nu}_{av} = 0.2(\mathrm{Ra}_{ri})^{0.174}(1 - 0.525L)[1 + 28.01(R - 1)]: \quad 1 \times 10^5 \leq \mathrm{Ra}_{ri} \leq 1 \times 10^6 \tag{36}$$

Wheel and Brake Assembly

The wheel and brake assembly internal flow regions are comprised of (a) a narrow gap brake stack/wheel annulus which is open to the ambient on the inboard end and bounded on the outboard end by the air space between the stack and wheel web, (b) a wide gap wheel outboard annular cavity which is open to the ambient on the outboard end, and (c) ventilation passages in the wheel web which connect the inboard and outboard regions as shown in Fig. 5. A numerical and experimental investigation of turbulent natural convection in this geometry has recently been performed and the results are introduced in this section. A test section representing the geometry shown in Fig. 5 was employed in the experimental part of this study. Experiments were performed over a range of Rayleigh numbers which encompasses most of the range of aircraft brake operating conditions. Temperature distributions within the wheel and brake components were recorded for use in development of average Nusselt number relations and validation of the numerical model. The numerical results were found to be in excellent agreement with the experimental data. Visualization of the natural convection flow patterns using incense smoke was also performed using the experimental test section. From these tests, the primary features of the flow field predicted by the numerical model were qualitatively verified. Nusselt number correlations for the brake stack were developed from the experimental results. These correlations are of the form

$$\mathrm{Nu}_{av} = A(\mathrm{Ra}^*_{ro})^B \tag{37}$$

where A and B vary from 0.091 to 0.154 and 0.256 to 0.281, respectively, depending on the Rayleigh number range.

In the numerical portion of the investigation, an extended computational domain was utilized to implement the virtually unknown boundary conditions at the open ends. The governing equations (Eqs. (10)–(15)) and the relevant boundary conditions were discretized using a finite element formulation based on the Galerkin method of weighted residuals. The system of discretized equations was solved using a segregated approach in which the global matrix is decomposed into smaller submatrices each associated with only one of the independent variables. The submatrices were solved sequentially using the conjugate gradient and conjugate residual methods for the nonsymmetric and symmetric equation systems, respectively. Convergence of these iterative schemes was assumed to have been achieved when the relative change of each independent variable between successive iterations was less than 0.001.

To ensure the numerical results were not dependent on the grid size, a mesh refinement procedure was adopted in which results for different grid distributions were compared. In this procedure, the number of grid points in the radial direction was first successively increased while the angular and axial grid points were held constant. Keeping the number of axial grid points the same, the number of angular grid points was then successively increased using the grid size in the radial direction obtained from the previous step. With the angular and radial grid sizes thus established, the number of grids in the axial direction was then successively increased. Finally, the number of grids in all three directions were increased to determine the grid size which yielded grid-independent results.

A constant heat flux was applied to the thermally conductive solid elements which form the cylindrical wall and vertical end faces of the brake stack to represent the heat generation within the stack. A reduced value of heat flux was applied to the conductive aluminum wheel elements to account for heating of the wheel by conduction and radiation from the brake stack. To a very reasonable approximation, the aircraft tire surface can be considered to be adiabatic. Therefore, in the numerical model Eq. (21) was applied at the vertical surfaces of the tire facing the open flow region.

The natural convection flow is driven by the temperature differences between the heated surfaces of the wheel and brake assembly and the cooler ambient air. Heat is transferred from these surfaces to air within the internal passageways of the assembly, which produces convective currents due to density gradients which arise in the air. The heated vertical surfaces of the brake stack and wheel hub that are exposed directly to the ambient air induce currents external to the assembly which interact with the air leaving the inboard and outboard annular openings. Particle paths obtained from the numerical model are shown in Figs. 6 and 7 for a Rayleigh number of $\mathrm{Ra}^*_{ro} = 3 \times 10^9$. These paths represent the trajectories of massless fluid particles injected into the flow field immediately outside the brake stack/wheel and wheel outboard cavities at positions within the lower (Fig. 6) and middle to upper regions (Fig. 7) of these cavities. The radial positions of the particle release points ($0.55 \le r \le 1.1$, $\Delta r = 0.05$ at the inboard end and $0.1 \le r \le 1.1$, $\Delta r = 0.1$ at the outboard end) were chosen to encompass the annular opening and heated vertical surface at each end of the assembly. In Fig. 6, the particles which enter the lower portion of the brake stack/wheel annulus or wheel outboard cavity are numbered. It should be noted that the letters a and b designate the release points and end positions, respectively, of the particles. For example, 1a is the release point of particle 1 and 1b is the end position of particle 1. In Figs. 6–8, the physical boundary between the fluid and solid domains is superimposed on the numerical results. In the following discussion of results, the angular position θ is based on a cylindrical coordinate system in which the z-direction corresponds to the axis of the brake stack and $\theta = 0$ deg is at the uppermost vertical location (see Fig. 5).

As seen in Fig. 6(a), the suction mechanism draws air axially inward through the brake stack/wheel annulus aperture plane at $\theta = 160$ deg. One of the particles entering the annulus (particle 5) is seen to eventually become entrained in the circumferentially upward flow in the annulus, while the other particles (1, 2, 3, and 4) continue inward until reaching the gap between the brake stack and wheel web, and then rise circumferentially upward along the wheel web. In the upper part of this gap, two of the particles (1 and 2) enter the $\theta = 0$ deg wheel web ventilation passage and are ejected from the wheel outboard cavity in a buoyant stream. The other two particles (3 and 4) pass through the $\theta = 40$ deg ventilation passage and then become entrained in the fluid leaving the top of the wheel outboard cavity. The single particle remaining on the inboard side (particle 5) rises circumferentially in the space between the brake stack and wheel, reverses axial direction, and then proceeds to the brake stack/wheel annulus aperture plane where it is ejected from the top of the annulus in another buoyant stream. The particles introduced at the inboard end of the assembly at $\theta = 160$ deg which do not enter the annulus (for $0.55 \le r \le 0.85$) become entrained in the boundary layer rising along the vertical heated face of the brake stack (Fig. 6(a)). This air curves around the obstructing axle surface, rises above the axle in a buoyant plume, and becomes entrained in the air exiting the top of the brake stack/wheel annulus.

The air entering the wheel outboard cavity at $\theta = 160$ deg is drawn axially inward due to the suction mechanism as seen in Fig. 6(b). Part of this air (particles 8, 9, 10, and 11) is drawn through the $\theta = 160$ deg ventilation passage, where it subsequently gains energy from the heated brake stack and rises circumferentially upward. Most of this air continues until reaching the upper part of the brake stack, at which point it proceeds axially inboard through the brake stack/wheel gap until finally exiting on the inboard side of the assembly (particles 8, 9, and 10). A smaller portion of the air, however, flows back into the wheel outboard cavity through the $\theta = 0$ deg wheel ventilation passage, and then exits the cavity (particle 11). The air which enters the wheel outboard cavity at $\theta = 160$ deg but does not pass through any of the ventilation passages (particles 6, 7, and 12) becomes entrained in the boundary layers along the wheel outboard cavity surfaces and rises to the top region of the cavity before exiting to the ambient. As shown in Fig. 6(b), the air rising alongside the heated vertical face of the wheel hub is drawn slightly inward toward the wheel web due to the local suction effect above the hub. It continues upward and becomes entrained in the buoyant air stream leaving the $\theta = 0$ deg wheel web passage.

The air entering the brake stack/wheel annular gap at $\theta = 140$ deg (Fig. 6(c)) does not penetrate quite as far axially as that entering at $\theta = 160$ deg (Fig. 6(a)). As a result, all of the particles entering the brake stack/wheel gap at $\theta = 140$ deg (particles 13, 14, 15, 16, and 17) rise circumferentially to the top of the gap and then proceed in the opposite axial direction until exiting the annulus. Thus, it is seen from Figs. 6(a) and 6(c) that as the angular position of the particle release point is decreased from $\theta = 160$ deg to $\theta = 140$ deg, the particles *originating* from the inboard side no longer cross over to the outboard side through the upper ventilation passages.

The portion of air entering the wheel outboard cavity at $\theta = 140$ deg which crosses over to the inboard side of the wheel web (particles 21, 22, and 23) does so through the $\theta = 120$ deg ventilation passage as seen in Fig. 6(d). Instead of most of this air exiting the brake stack/wheel annulus on the inboard side, as it does when introduced at $\theta = 160$ deg (Fig. 6(b)),

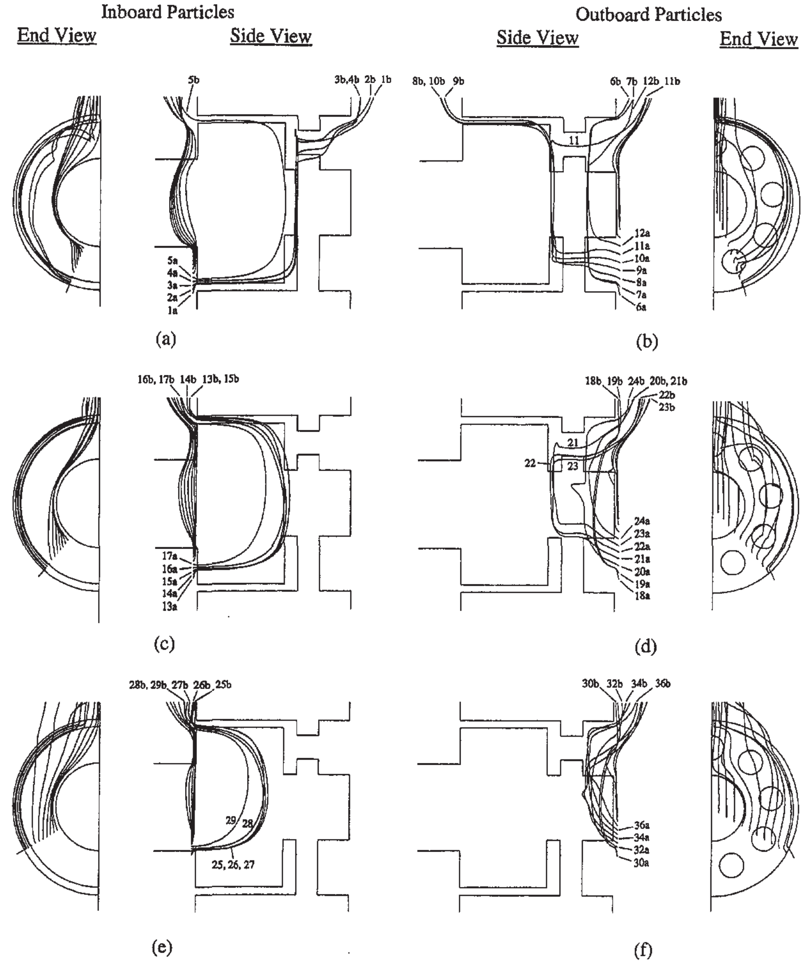

Fig. 6 Trajectories of particles released in the lower portion of the braking system inboard and outboard regions at (*a*) and (*b*) θ = 160 deg, (*c*) and (*d*) θ = 140 deg, and (*e*) and (*f*) θ = 120 deg for $Ra^*_{ro} = 3 \times 10^9$

all of the air now crosses back over to the wheel outboard cavity through the $\theta = 0$ deg (particle 21) and $\theta = 40$ deg (particles 22 and 23) passages (Fig. 6(*d*)). Therefore, it is seen that by reducing the outboard particle release point from $\theta = 160$ deg to $\theta = 140$ deg, the ensuing flow routes through the wheel web ventilation passages change dramatically.

With a further decrease in release position to $\theta = 120$ deg, the axial penetration of particles introduced on the inboard side of the assembly (particles 25, 26, 27, 28, and 29) decreases further, as seen in Fig. 6(*e*). The air entering the wheel outboard cavity at $\theta = 120$ deg no longer passes through any of the ventilation passages (Fig. 6(*f*)). Instead, all of this air becomes entrained in the boundary layers on the wheel surfaces, rises upward, and exits the cavity.

The trajectories of particles released at $\theta = 90$ deg, 60 deg, and 30 deg are shown in Figs. 7(*a*), 7(*b*), and 7(*c*), respectively. As the circumferential release point is decreased from $\theta = 120$ deg to $\theta = 90$ deg, the axial penetration of both the inboard and outboard particles diminishes even further as seen by comparing Figs. 6(*e*) and 6(*f*) with Fig. 7(*a*). In Fig. 7(*a*), it is seen that the air rising along the vertical face of the brake stack does not enter the brake stack/wheel annulus at angular positions less than approximately $\theta = 60$ deg. The air entering between $\theta = 90$ deg and $\theta = 60$ deg travels a relatively short distance before exiting near the top of the annular gap. Particles introduced at angular positions of $\theta = 60$ deg and $\theta = 30$ deg do not enter the brake stack/wheel annulus but rise past the open end instead, as seen in Figs. 7(*b*) and 7(*c*), respectively. On the outboard side of the assembly at $\theta = 60$ deg, ambient air penetrates into the wheel cavity only a small distance before reversing axial direction and exiting the wheel outboard cavity (Fig. 7(*b*)). At $\theta = 30$ deg, the ambient air no longer enters the wheel outboard cavity (Fig. 7(*c*)). As seen in Figs. 6 and 7, the ventilation passages in the wheel web are utilized only by the air originally entering the lower portions of the braking system inboard and outboard annular openings.

A vector plot of the natural convection velocity field at the angular symmetry plane is provided in Fig. 8(*a*) for $Ra^*_{ro} = 3 \times 10^9$. The local influx of ambient air into the bottom of the brake stack/wheel annulus and the velocity profiles of air flowing axially through the bottom of this annulus are clearly seen. As this air progresses toward the outboard end of the brake stack, the axial velocity decreases due to some of the air becoming entrained in the circumferentially upward flow in the annulus. At the top of the annulus, a stagnant region is seen to be present near the outboard end of the stack. On the inboard side of this stagnant region, the axial velocity increases rapidly with decreasing distance from the annulus inboard opening as more of the air rising in the annulus collects at the top and proceeds toward the opening. The air exits the top of the brake stack/wheel annulus in a high-speed buoyant jet, which entrains the heated air rising from the upper vertical face of the stack. On the outboard side of the stagnant region, the air in the top portion of the gap between the brake stack and wheel web enters the uppermost wheel web ventilation passage and then exits the entire assembly as a high speed buoyant jet of air. The air at

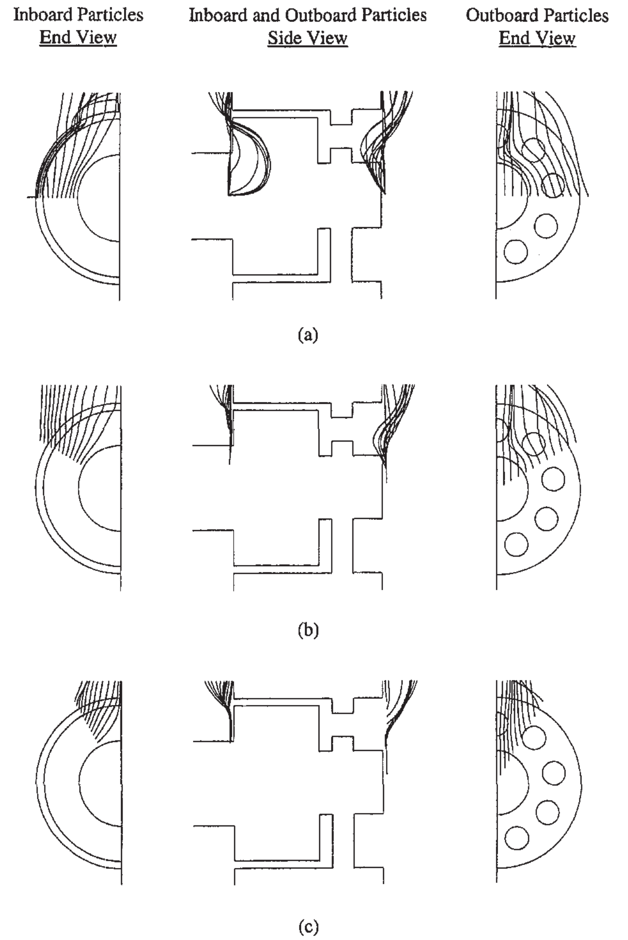

Fig. 7 Trajectories of particles released in the middle and upper portions of the braking system inboard and outboard regions at (*a*) $\theta = 90$ deg, (*b*) $\theta = 60$ deg, and (*c*) $\theta = 30$ deg for $Ra^*_{ro} = 3 \times 10^9$

the top of the wheel outboard cavity and that rising from the surfaces of the wheel hub become entrained in this jet. The buoyant jet at the upper portion of the brake stack/wheel annulus, which is characteristic of open cavity flows, and that exiting from the uppermost wheel web ventilation passage are the most prominent features of the braking system flow field.

The isotherms in the angular symmetry plane calculated numerically for $Ra^*_{ro} = 3 \times 10^9$ are shown in Fig. 8(*b*). The suction of cold ambient air into the bottom of the brake stack/wheel annulus and the increasing thermal boundary layer thickness as the air proceeds axially toward the end of the brake stack are evident in the isotherms. The inflow of cold air from the annulus into the gap between the brake stack and wheel web is also apparent. The increase in thermal boundary layer thickness along the lower part of the brake stack vertical surface facing the inboard ambient region and along the wheel hub vertical surface facing the outboard ambient region is distinctly seen. The significant distortion of isotherms adjacent to the top of the brake stack/wheel annulus open end reflect the presence of the buoyant jet leaving the annulus. Likewise, at the top of the outboard end of the assembly the distorted isotherms are indicative of the buoyant jet leaving the uppermost wheel web ventilation passage. The isotherms next to the surfaces in the bottom of the brake stack/wheel annulus and the bottom of the wheel outboard cavity are spaced relatively close together compared to corresponding locations at the top of the assembly. This is indicative of the higher heat transfer rates at the bottom locations which results from thermal boundary layer development and the increase in bulk temperature of the air as it rises within the heated annular regions of the assembly. The numerically calculated temperatures of the wheel and brake components were found to be in excellent agreement with those obtained experimentally.

Based on the presented detailed aspects of the flow field and temperature distribution, a number of overall attributes can be cited. For example, it has been determined that ambient air is drawn into the narrow gap brake stack/wheel annulus and large gap wheel outboard annular cavity over roughly the lower two-thirds of the open ends, and heated air is ejected to the ambient across approximately the upper one-third of these openings. This was confirmed by plotting the axial velocities at the inboard and outboard aperture planes. Since the incoming air occupies a much larger segment of the annulus opening than the outgoing air, its velocity is lower due to conservation of mass. It was shown that a portion of the ambient air entering the bottom of the brake stack/wheel and wheel outboard annular openings flows through the wheel web ventilation passages, while the air entering in the

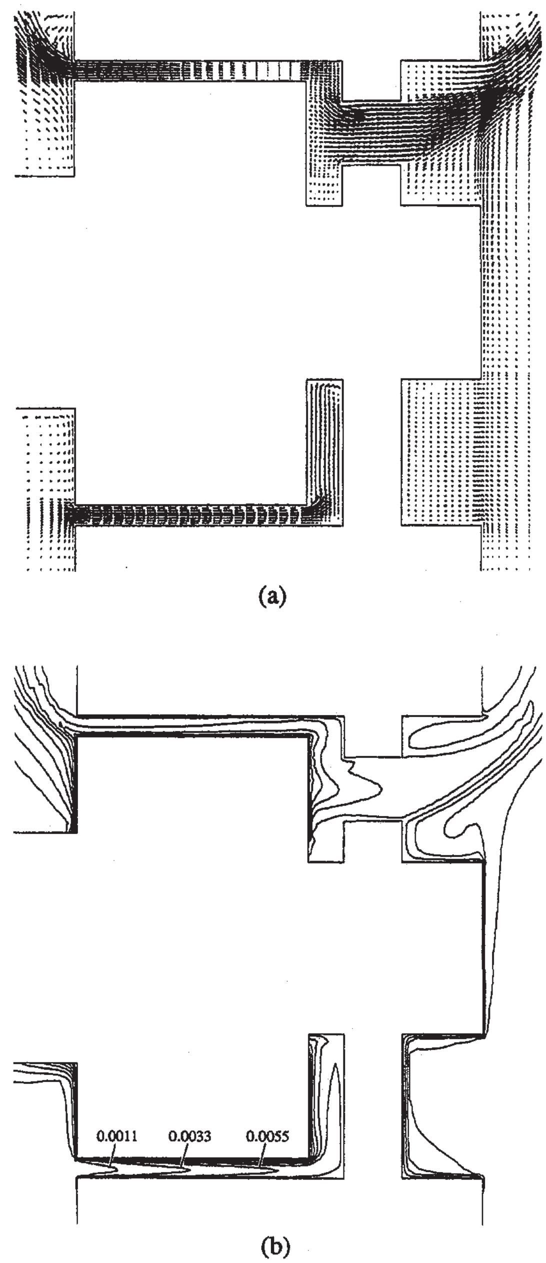

Fig. 8 Natural convection in the angular symmetry plane for $Ra^*_{ro} = 3 \times 10^9$; (*a*) velocity field, (*b*) isotherms

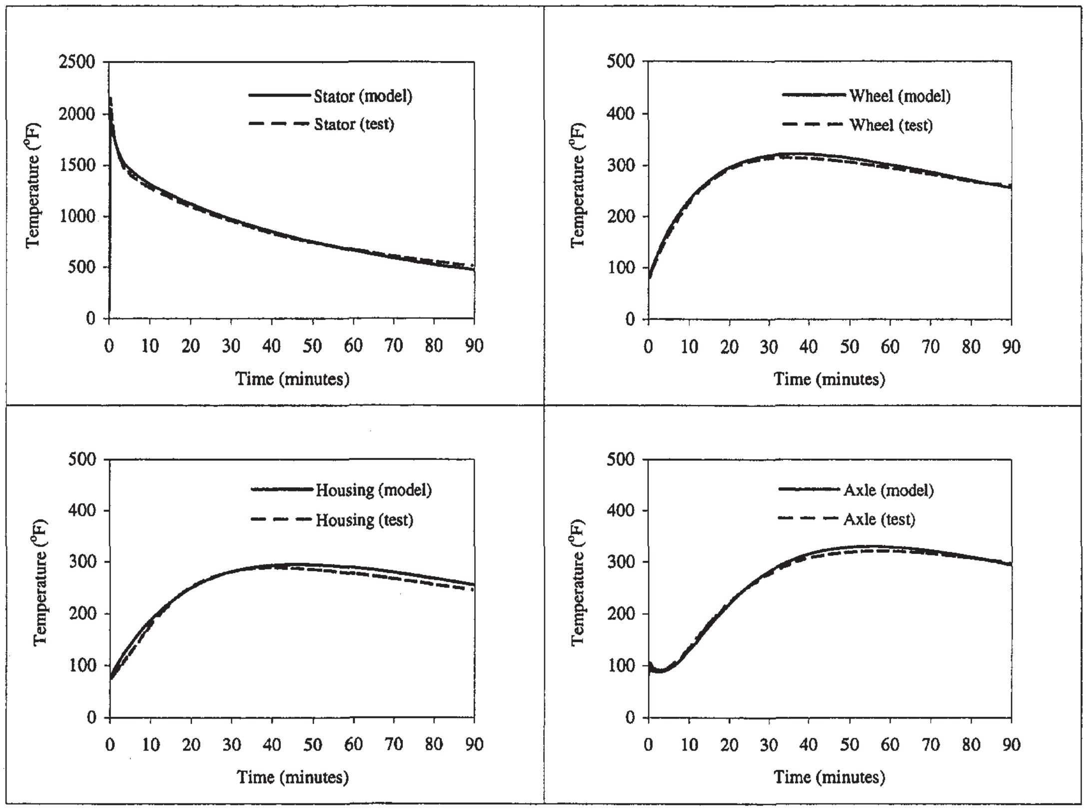

Fig. 9 Comparison of calculated temperature responses of aircraft braking system components with experimental data

middle portion of these openings does not. The primary features of the braking system natural convection flow field seen in the numerical results were confirmed in the flow visualization studies, where the previously described air inflow and outflow boundaries, strong buoyant outflow of air at the top of the annular cavities, and crossover of air from the outboard to inboard and inboard to outboard sides of the wheel web were observed.

The results of the experimental and numerical investigations of the wheel and brake assembly domain and the braking system subdomains were utilized to develop convective heat transfer coefficient relationships for different regions of the braking system as a function of Rayleigh number and the primary geometric parameters. These relationships were integrated into a braking system thermal analysis code developed and employed by Aircraft Braking Systems Corporation. An example of results obtained from this code using the convection coefficient relationships is presented in Fig. 9, which shows the calculated temperature responses of critical components of the aircraft wheel and brake after a braking event. Measured temperature responses obtained from a dynamometer test using full-scale braking system hardware are also plotted in Fig. 9. The braking system thermal model results are seen to be in excellent agreement with the experimental data, further verifying the convective heat transfer results from the studies of the wheel and brake assembly domain and braking system subdomains.

Summary

This work has discussed the practical significance of the brake cooling problem and has reviewed both fundamental considerations and recent developments in analysis of aircraft brake natural convection. The recent investigations of geometries and thermal conditions relevant to the aircraft braking system have arisen from a nearly complete absence of studies focused on this application only a decade ago. Numerical simulations of the wheel and brake assembly natural convection flow field have been developed and are now being utilized in industry for cooling optimization, thereby reducing the need for costly experimentation. A great deal has been learned about the characteristics of the buoyancy-induced flow and heat transfer, and progress has been made toward defining more efficient thermal designs. However, there are still unanswered questions concerning enhanced cooling design trade-offs and the effects of more detailed geometric features on cooling performance. It is expected that this will foster considerable continuing activity in this field.

The presented numerical and experimental investigation has established in detail the basic structure of natural convection flow within the aircraft wheel and brake assembly and shown that the physical mechanisms underlying buoyancy-induced flow in basic open-ended annuli are also strongly present in the braking system. The bulk flow is characterized by suction of air into the middle and lower regions of the narrow gap brake stack/wheel annulus and wide gap wheel outboard annular cavity, overall upward movement as the air is heated by the brake stack and wheel surfaces, outflow of air over roughly the top one-third of the inboard and outboard annular openings, and ejection of hot air from the top of the brake stack/wheel annulus and uppermost wheel web ventilation passage in separate strong buoyant jets. The wheel web ventilation passages connecting the inboard and outboard regions are utilized only by the air originally entering the bottom of the inboard and outboard annular openings. The primary features of the flow field and the temperature distribution in the wheel and brake components resulting from the buoyancy-induced flow were verified experimentally. Results of the numerical and experimental investigation were utilized to develop convective heat transfer relationships for different regions of the braking system. The results from a thermal model of the braking system which employed these relationships were found to be in excellent agreement with experimental data obtained from full scale braking system hardware.

Acknowledgments

The authors gratefully acknowledge and appreciate the support of Aircraft Braking Systems Corporation for the past few years.

References

Abib, A. H., and Jaluria, Y., 1988, ''Numerical Simulation of the Buoyancy-Induced Flow in a Partially Open Enclosure,'' *Numerical Heat Transfer,* Vol. 14, pp. 235–254.

Bejan, A., and Kimura, S., 1981, ''Penetration of Free Convection Into a Lateral Cavity,'' *Journal of Fluid Mechanics,* Vol. 103, pp. 465–478.

Bishop, E. H., and Carley, C. T., 1966, ''Photographic Studies of Natural Convection Between Concentric Cylinders,'' *Proceedings of the 1966 Heat Transfer and Fluid Mechanics Institute,* pp. 63–78.

Bishop, E. H., 1988, ''Heat Transfer by Natural Convection of Helium Between Horizontal Isothermal Concentric Cylinders at Cryogenic Temperature,'' ASME JOURNAL OF HEAT TRANSFER, Vol. 110, pp. 109–115.

Braun, M. J., Daniels, C. C., Dyko, M. P., and Krga, V., 1997, ''Temperature Distribution and Flow Characteristics of a Concentric Horizontal Cylinder Configuration,'' *Proceedings of the 1997 ASME Fluids Engineering Division Summer Meeting,* Paper No. FEDSM-3088.

Chan, Y. L., and Tien, C. L., 1983, ''Laminar Natural Convection in Shallow Open Cavities,'' *Natural Convection in Enclosures,* HTD-Vol. 26, ASME, New York, pp. 77–82.

Chan, Y. L., and Tien, C. L., 1985a, ''A Numerical Study of Two-Dimensional Natural Convection in Square Open Cavities,'' *Numerical Heat Transfer,* Vol. 8, pp. 65–80.

Chan, Y. L., and Tien, C. L., 1985b, ''A Numerical Study of Two-Dimensional Laminar Natural Convection in Shallow Open Cavities,'' *International Journal of Heat and Mass Transfer,* Vol. 28, pp. 603–612.

Chan, Y. L., and Tien, C. L., 1986, ''Laminar Natural Convection in Shallow Open Cavities,'' ASME JOURNAL OF HEAT TRANSFER, Vol. 108, pp. 305–309.

Clark, S. K., and Dodge, R. N., 1984, ''Heat Generation in Aircraft Tires Under Braked Rolling Conditions,'' NASA Contractor Report 3768.

Currey, N. S., 1988, ''Aircraft Landing Gear Design: Principles and Practices,'' AIAA Education Series, pp. 137–173.

Desai, C. P., and Vafai, K., 1992, ''Three-Dimensional Buoyancy Induced Flow and Heat Transfer Around the Wheel Outboard of an Aircraft,'' *International Journal of Heat and Fluid Flow,* Vol. 13, pp. 50–64.

Desai, C. P., and Vafai, K., 1993, ''Investigation of the Temporal Thermal Performance of the Wheel Outboard of an Aircraft,'' *Journal of Thermophysics and Heat Transfer,* Vol. 7, pp. 377–384.

Desai, C. P., and Vafai, K., 1994, ''An Investigation and Comparative Analysis of Two- and Three-Dimensional Turbulent Natural Convection in a Horizontal Annulus,'' *International Journal of Heat and Mass Transfer,* Vol. 37, pp. 2475–2504.

Desai, C. P., and Vafai, K., 1996, ''Experimental and Numerical Study of Buoyancy-Induced Flow and Heat Transfer in an Open Annular Cavity,'' *International Journal of Heat and Mass Transfer,* Vol. 39, pp. 2053–2066.

Desai, C. P., Vafai, K., and Dyko, M. P., 1996, ''Heat Transfer Optimization Within Open-Ended Annular Cavities,'' *Journal of Thermophysics and Heat Transfer,* Vol. 11, pp. 121–124.

Dyko, M. P., and Chung, B. T. F., 1990, ''Finite Element Thermal Model of an Aircraft Wheel and Carbon Brake Assembly,'' *SAE Transactions, Journal of Aerospace,* Paper No. 901909.

Dyko, M. P., Vafai, K., and Mojtabi, A. K., 1999, ''A Numerical and Experimental Investigation of Stability of Natural Convective Flows Within a Horizontal Annulus,'' *Journal of Fluid Mechanics,* in press.

Ettefagh, J., and Vafai, K., 1988, ''Natural Convection in Open-Ended Cavities With a Porous Obstructing Medium,'' *International Journal of Heat and Mass Transfer,* Vol. 31, pp. 673–693.

Ettefagh, J., and Vafai, K., 1991, ''An Investigation of Ejection, Mixing, and Suction Mechanisms in an Open-Ended Horizontal Annulus,'' ASME JOURNAL OF HEAT TRANSFER, Vol. 113, pp. 1025–1028.

Ettefagh, J., Vafai, K., and Kim, S. J., 1991, ''Non-Darcian Effects in Open-Ended Cavities Filled With a Porous Medium,'' ASME JOURNAL OF HEAT TRANSFER, Vol. 113, pp. 747–756.

Farouk, B., and Guceri, S. I., 1982, ''Laminar and Turbulent Natural Convection in the Annulus Between Horizontal Concentric Cylinders,'' ASME JOURNAL OF HEAT TRANSFER, Vol. 104, pp. 631–636.

Fukuda, K., Yasutomi, M., and Hasegawa, S., 1990, ''Analytical and Experimental Study on Turbulent Natural Convection in a Horizontal Annulus,'' *International Journal of Heat and Mass Transfer,* Vol. 33, pp. 629–639.

Fukuda, K., Yasutomi, M., Taniguchi, N., Morita, K., and Hasegawa, S., 1991, ''Direct Simulation and Large Eddy Simulation of Turbulent Natural Convection in Horizontal Annulus,'' *Memoirs of Faculty of Engineering–Kyushu University,* Vol. 51, pp. 355–369.

Fusegi, T., and Farouk, B., 1986, ''A Three-Dimensional Study of Natural Convection in the Annulus Between Horizontal Concentric Cylinders,'' *Proceedings of the Eighth International Heat Transfer Conference,* Vol. 4, pp. 1575–1580.

Greenbank, S. J., 1991, ''Landing Gear–The Aircraft Requirement,'' *Proceedings of The Institution of Mechanical Engineers, Part G: Journal of Aerospace Engineering,* Vol. 205, pp. 27–34.

Grigull, U., and Hauf, W., 1966, ''Natural Convection in Horizontal Cylindrical Annuli,'' *Proceedings of the Third International Heat Transfer Conference,* Vol. 2, pp. 182–195.

Haroutunian, V., and Engelman, M. S., 1991, ''On Modeling Wall-Bound Turbulent Flows Using Specialized Near-Wall Finite Elements and the Standard $k-\varepsilon$ Model,'' *Advances in Numerical Simulation of Turbulent Flows,* FED-Vol. 117, ASME, New York, pp. 97–105.

Hess, C. F., and Henze, R. H., 1984, ''Experimental Investigation of Natural Convection Losses From Open Cavities,'' ASME JOURNAL OF HEAT TRANSFER, Vol. 106, pp. 333–338.

Humphrey, J. A. C., and To, W. M., 1986, ''Numerical Simulation of Buoyant, Turbulent Flow–II. Free and Mixed Convection in a Heated Cavity,'' *International Journal of Heat and Mass Transfer,* Vol. 29, pp. 593–610.

Iyer, S. V., and Vafai, K., 1997, ''Effects of a Geometric Perturbation on Buoyancy Induced Flow and Heat Transfer in a Cylindrical Annulus,'' *International Journal of Heat and Mass Transfer,* Vol. 40, pp. 2901–2911.

Iyer, S. V., and Vafai, K., 1998, ''Buoyancy Induced Flow and Heat Transfer in a Cylindrical Annulus With Multiple Perturbations,'' *International Journal of Heat and Mass Transfer,* Vol. 41, pp. 3025–3035.

Kuehn, T. H., and Goldstein, R. J., 1976, ''An Experimental and Theoretical Study of Natural Convection in the Annulus Between Horizontal Concentric Cylinders,'' *Journal of Fluid Mechanics,* Vol. 74, pp. 695–719.

Kuehn, T. H., and Goldstein, R. J., 1978, ''An Experimental Study of Natural Convection Heat Transfer in Concentric and Eccentric Horizontal Cylindrical Annuli,'' ASME JOURNAL OF HEAT TRANSFER, Vol. 100, pp. 635–640.

Le Quere, P., Humphrey, J. A. C., and Sherman, F. S., 1981, ''Numerical Calculation of Thermally Driven Two-Dimensional Unsteady Natural Convection Flow in Cavities of Rectangular Cross-Section,'' *Numerical Heat Transfer,* Vol. 4, pp. 249–283.

Liu, C., Mueller, W. K., and Landis, F., 1961, ''Natural Convection Heat Transfer in Long Horizontal Cylindrical Annuli,'' *International Developments in Heat Transfer,* Part V, pp. 976–984.

Mahoney, D. N., Kumar, R., and Bishop, E. H., 1986, ''Numerical Investigation of Variable Property Effects on Laminar Natural Convection of Gases Between Two Horizontal Isothermal Concentric Cylinders,'' ASME JOURNAL OF HEAT TRANSFER, Vol. 108, pp. 783–789.

McLeod, A. E., and Bishop, E. H., 1989, ''Turbulent Natural Convection of Gases in Horizontal Cylindrical Annuli at Cryogenic Temperatures,'' *International Journal of Heat and Mass Transfer,* Vol. 32, pp. 1967–1978.

Miyamoto, M., Kuehn, T. H., Goldstein, R. J., and Katoh, Y., 1989, ''Two-Dimensional Laminar Natural Convection Heat Transfer From a Fully or Partially Open Square Cavity,'' *Numerical Heat Transfer,* Part A, Vol. 15, pp. 411–430.

Mohamad, A. A., 1995, ''Natural Convection in Open Cavities and Slots,'' *Numerical Heat Transfer,* Part A, Vol. 27, pp. 705–716.

Morita, K., Nakamura, Y., Taniguchi, N., Fukuda, K., and Hasegawa, S., 1990, ''Unsteady Three-Dimensional Behavior of Natural Convection in Horizontal Annulus–Validity of Direct Numerical Simulation of Turbulent Natural Convection,'' *Journal of the Atomic Energy Society of Japan,* Vol. 32, pp. 719–727.

Ozoe, H., Okamato, T., and Churchill, S. W., 1979, ''Natural Convection in a Vertical Annular Space Heated From Below,'' *Heat Transfer–Japanese Research,* Vol. 8, pp. 82–93.

Ozoe, H., Shibata, T., and Churchill, S. W., 1981, ''Natural Convection in an Inclined Circular Cylindrical Annulus Heated and Cooled On Its End Plates,'' *International Journal of Heat and Mass Transfer,* Vol. 24, pp. 727–737.

Penot, F., 1982, ''Numerical Calculation of Two-Dimensional Natural Convection in Isothermal Open Cavities,'' *Numerical Heat Transfer,* Vol. 5, pp. 421–437.

Powe, R. E., Carley, C. T., and Bishop, E. H., 1969, ''Free Convective Flow Patterns in Cylindrical Annuli,'' ASME JOURNAL OF HEAT TRANSFER, Vol. 91, pp. 310–314.

Rao, Y. F., Miki, Y., Fukuda, K., Takata, Y., and Hasegawa, S., 1985, ''Flow Patterns of Natural Convection in Horizontal Cylindrical Annuli,'' *International Journal of Heat and Mass Transfer,* Vol. 28, pp. 705–714.

Skok, H., Ramadhyani, S., and Schoenhals, R. J., 1991, ''Natural Convection in a Side-Facing Open Cavity,'' *International Journal of Heat and Mass Transfer,* Vol. 12, pp. 36–45.

Takata, Y., Iwashige, K., Fukuda, K., and Hasegawa, S., 1984, ''Three-Dimensional Natural Convection in An Inclined Cylindrical Annulus,'' *International Journal of Heat and Mass Transfer,* Vol. 27, pp. 747–754.

Vafai, K., and Ettefagh, J., 1990a, ''The Effects of Sharp Corners on Buoyancy-Driven Flows with Particular Emphasis on Outer Boundaries,'' *International Journal of Heat and Mass Transfer,* Vol. 33, pp. 2311–2328.

Vafai, K., and Ettefagh, J., 1990b, ''Thermal and Fluid Flow Instabilities in Buoyancy-Driven Flows in Open-Ended Cavities,'' *International Journal of Heat and Mass Transfer,* Vol. 33, pp. 2329–2344.

Vafai, K., and Ettefagh, J., 1991a, ''An Investigation of Transient Three-Dimensional Buoyancy-Driven Flow and Heat Transfer in a Closed Horizontal Annulus,'' *International Journal of Heat and Mass Transfer,* Vol. 34, pp. 2555–2570.

Vafai, K., and Ettefagh, J., 1991b, ''Axial Transport Effects on Natural Convection Inside of an Open-Ended Annulus,'' ASME JOURNAL OF HEAT TRANSFER, Vol. 113, pp. 627–634.

Vafai, K., Desai, C. P., Iyer, S. V., and Dyko, M. P., 1997, ''Buoyancy-Induced Convection in a Narrow Open-Ended Annulus,'' ASME JOURNAL OF HEAT TRANSFER, Vol. 119, pp. 483–494.